

Wintertime variability in the Euro–Atlantic region in observations and in ECMWF seasonal ensemble experiments

By V. PAVAN¹*, F. MOLTENI² and Č. BRANKOVIĆ³

¹*University of Bologna, Italy*

²*CINECA—Interuniversity Computing Centre, Bologna, Italy*

³*European Centre for Medium-Range Weather Forecasts, UK*

(Received 23 June 1998; revised 8 February 2000)

SUMMARY

An empirical orthogonal function (EOF) decomposition of monthly mean analyses of 500 hPa height (1949–94) is used to describe the interannual variability of the large-scale flow in the Euro–Atlantic region during winter. The first four EOFs resemble low-frequency variability patterns identified in previous studies, such as the North Atlantic Oscillation, and the eastern Atlantic and Eurasian teleconnection patterns. The second EOF and fourth EOF (EOF4) are associated with the occurrence of El Niño-like sea surface temperature (SST) anomalies according to an observational analysis; for EOF4, correlations with SST anomalies in the west Pacific are also important. Indications of an influence of tropical SST anomalies on the blocking-like third EOF, emerging from the European Centre for Medium-Range Weather Forecasts (ECMWF) re-analysis (ERA) data, are not confirmed by a longer SST record. A negligible correlation exists between the first EOF and El Niño indices during the ERA period, although a link may be detected in earlier decades.

In the second part of the paper, a 14-winter set of seasonal ensemble simulations, performed with the ECMWF atmospheric model forced by observed SST, is validated by comparing the projection of ERA data onto the four leading Euro–Atlantic EOFs with those of ensemble experiments, and computing composite anomalies of analyses and model fields. The performance of the model is uneven and depends on the large-scale pattern considered. Model biases and flow-dependent errors affect the simulations of some of the EOFs: In particular the model has strong problems reproducing the occurrence of European blocks. The best correlation (69%) between the time series of analysis and ensemble-mean principal components is obtained for EOF4, which seems to be forced by SST anomalies in the west Pacific associated with El Niño/Southern Oscillation (ENSO) events. The effects of this forcing are felt on the zonal wind structure over Eurasia, and are reasonably reproduced by the ECMWF model. Conversely, the propagation into the Atlantic region of planetary waves originating in the east Pacific is poorly simulated, thus degrading the model performance in predicting Euro–Atlantic anomalies during some strong ENSO events.

KEYWORDS: Ensemble simulations Euro–Atlantic variability Seasonal predictability

1. INTRODUCTION

The region including the North Atlantic and Europe is characterized by a large atmospheric variability on all time-scales. On periods which range from months to decades, the Euro–Atlantic variability is dominated by the so-called North Atlantic Oscillation (NAO) pattern, which is associated with a large-scale dipole in surface pressure with centres approximately over Iceland and the Azores (van Loon and Rogers 1978). Other important patterns of Euro–Atlantic low-frequency variability on monthly and seasonal scales have been described by Wallace and Gutzler (1981), Barnston and Livezey (1987) and Rogers (1990). Recently, much attention has been devoted to the interdecadal variations of NAO-like anomalies (Deser and Blackmon 1993; Kushnir 1994; Hurrell 1995, 1996). Possible explanations for variability on this time-scale (apart from possible climate trends associated with human activities) include oscillations of the thermohaline circulation in the North Atlantic (Delworth *et al.* 1993), or coupled oscillations involving the Atlantic sub-tropical gyre and storm-track (Latif *et al.* 1996).

On the other hand, the NAO and other Euro–Atlantic large-scale anomalies exhibit a substantial variability on scales between two and ten years (Hurrell and van Loon 1997), which may originate from different dynamical processes. Part of this variability may arise from the chaotic nature of the extra-tropical circulation, with no specific dynamical causes other than those which determine the intraseasonal variability in the region (see,

* Corresponding author: c/o CINECA, Via Magnanelli 6/3, Casalecchio di Reno, 40033 Bologna, Italy.

for example, the quasi-geostrophic simulations of NAO variability described by Molteni and Corti (1998)). A possible role of extra-tropical ocean–atmosphere interactions in the North Atlantic, first suggested by Ratcliff and Murray (1970), was supported by the response to North Atlantic sea surface temperature (SST) anomalies simulated in the modelling studies by Palmer and Sun (1985) and Ferranti *et al.* (1994a). However, recent studies by Cayan (1992) and Battisti *et al.* (1995) suggest that SST anomalies in the North Atlantic are mainly driven by anomalous heat fluxes induced by the atmospheric variability. The extra-tropical ocean feedback onto the atmospheric circulation could still cause a reddening of the spectrum of Euro–Atlantic atmospheric anomalies and, therefore, be a non-negligible source of intradecadal variability (e.g. Rodwell *et al.* 1999).

Although the extra-tropical processes mentioned above can be active in both the North Atlantic and north Pacific sector (see Latif *et al.* 1996), the situation in the two regions is remarkably different as far as tropical–extra-tropical interactions are concerned. While for the Pacific–North American (PNA) region a significant portion of interannual variability is known to arise from teleconnections with tropical anomalies associated with the El Niño/Southern Oscillation (ENSO), there is no firm observational evidence of a substantial influence of tropical SST anomalies on Euro–Atlantic interannual variability (e.g. Palmer and Anderson 1994). The direct influence of SST anomalies in the tropical Atlantic seems to be mostly limited to the tropical regions surrounding the ocean basin (Moura and Shukla 1981; Rao *et al.* 1993; Rowell *et al.* 1995). As far as ENSO is concerned, some statistically significant signals have been reported (Fraedrich and Muller 1992; Rodo' *et al.* 1997), but they only explain a small portion of the total interannual variability over Europe. On the other hand, general-circulation model (GCM) simulations of interannual variability forced by observed SST, such as those described by Molteni *et al.* (1993) and Branković *et al.* (1994), indicate a reproducible impact of at least some strong ENSO events over the Euro–Atlantic region.

The dynamical mechanism that leads to a response to Pacific SST anomalies in the European region is still to be properly understood. Theories of planetary-wave propagation such as those put forward by Hoskins and Karoly (1981) suggest that the Rossby-wave response to a forcing in the tropical Pacific would only reach Europe if some dynamical confinement prevented it from following a great-circle path into the tropical Atlantic, where it would be eventually dissipated. Alternatively, the nonlinear reflection of planetary waves investigated by Brunet and Haynes (1996) could be invoked as the source of a secondary response emerging from the tropical Atlantic, which could amplify the anomalies over the east Atlantic and Europe.

In this study, we will investigate the origin and predictability (given prescribed SSTs) of monthly and seasonal anomalies in the Euro–Atlantic region, by analysing the results of nine-member ensemble integrations of the European Centre for Medium-Range Weather Forecasts (ECMWF) GCM forced by observed SST (see Branković and Palmer 2000). These integrations were performed as part of the European Programme on Prediction of Climate Variations on Seasonal to Interannual Time-scales (PROVOST); they cover the 14-winter period (December through March) from 1979/80 to 1992/93, and use initial and boundary conditions from the ECMWF re-analysis (ERA) (Gibson *et al.* 1997).

The paper is organized as follows. Section 2 provides a detailed description of the data and the analysis methodology. In section 3, the leading patterns of Euro–Atlantic wintertime variability on the monthly-to-seasonal time-scale will be defined by an empirical orthogonal function (EOF) analysis of observed monthly means of 500 hPa height over a 45-year period. In section 4, links between the leading atmospheric EOFs

and SST anomalies will be investigated, with particular emphasis on the 1980–93 period covered by the ECMWF integrations. In section 5, the performance of the ECMWF model in simulating the variability associated with the leading EOFs will be analysed by comparing statistics of observed and modelled principal components (PCs), and fields of composite anomalies. In section 6, the results will be discussed and interpreted using dynamical indices of planetary-wave forcing and propagation, and conclusions will be drawn in section 7.

2. DATA AND DIAGNOSTIC TOOLS

(a) *Datasets for observational analyses*

In the observational part of this paper, diagnostic analyses are performed on a series of 500 hPa geopotential-height fields from 1949 to 1994, extracted from the US National Meteorological Center (NMC), currently National Centers for Environmental Prediction (NCEP), operational-analysis archives. The data are available twice daily, apart from a few gaps, on the NCEP octagonal grid including 1977 grid points from 20°N to the north pole. Before applying the diagnostic tools the data were interpolated onto a 2.5° × 2.5° regular grid.

Relationships between 500 hPa height anomalies, SST and precipitation data are investigated using the following datasets:

- Monthly-mean SSTs from ERA (Gibson *et al.* 1997), covering the 15-year period 1979–1993, which are derived from the global sea ice coverage and SST data compiled at The Met. Office (Parker *et al.* 1995) up to October 1981, and from the NCEP optimum-interpolation SST analysis (Reynolds and Smith 1994) after that.
- Monthly mean SSTs for the period 1950–92, compiled at NCEP using an EOF-based reconstruction method (Smith *et al.* 1996), which are available on a 2° × 2° regular grid.
- Monthly mean precipitation estimates by Xie and Arkin (1996), obtained by merging monthly rain-gauge observations and several estimates based on satellite data, and available from 1979 to 1995 on a 2.5° × 2.5° regular grid.

(b) *Empirical orthogonal function analysis*

The first step of our study is a standard EOF analysis on the time series of monthly averaged 500 hPa geopotential-height anomalies, focussed on the extended winter season (December, January, February and March) from 1949/50 to 1993/94. The target area for the EOF computation is the region from 20°N to 90°N and from 90°W (close to the east coast of North America) to 60°E (east of the Caspian Sea).

The time series of standardized principal components (PCs) obtained by projecting the monthly anomalies onto the EOFs are the basis of the present study. Specifically, we concentrate on the PCs associated with the four leading EOFs (EOF1, EOF2, EOF3, and EOF4), which together explain more than 50% of the total variance of the 500 hPa geopotential height. They will be used as a benchmark to verify the ECMWF winter ensemble forecasts in the second half of the paper.

The correlation of these PCs with the frequency of major European weather regimes, such as Atlantic blocking and European blocking, and with the cyclone frequency in the Atlantic storm-track will be discussed elsewhere (Pavan *et al.* 2000).

(c) *The ECMWF winter ensembles and their validation*

In the second part of the paper, we estimate the predictability of the Euro–Atlantic anomalies, represented by the leading EOFs, by analysing how these anomalies are simulated in a set of ensemble integrations of the ECMWF model forced by observed SSTs.

The winter ensemble set includes 14 years of ensemble integrations covering the (December to March) winters from 1979/80 to 1992/93. Each ensemble consists of nine integrations, started on consecutive days from 22 to 30 November. The model used for these integrations is the 13r4 version of the ECMWF atmospheric GCM, run at T63 spectral truncation and with 31 vertical levels. The integrations are forced by observed SST from ERA (see section 2(a) above, and Branković and Palmer (2000) for more details); initial conditions are also taken from the re-analysis.

The verifications of these ensembles were limited to the months of January, February and March (JFM); in this period, the nine ensemble members can be considered as independent, since the influence of initial conditions should be negligible after more than one month of integration. The validation is performed using ERA, except for precipitation fields which are compared with estimates from Xie and Arkin (1996).

The first step of the validation is the comparison of seasonal (JFM) means of Euro–Atlantic PCs (i.e. projections on EOFs) from analysis and model fields. Usually, seasonal rather than monthly averages are used for the validation of SST-forced integrations, since they are supposed to provide a stronger filtering of the unpredictable component of the circulation. However, the response to a given SST anomaly may be seasonally dependent (e.g. Peng *et al.* 1995), and different ways of averaging are possible.

An alternative way to validate the model integrations is to compute composites of observed and model anomalies in all months in which the observed value of a given PC exceeds a certain positive or negative threshold, and then take the difference between the positive and negative composites. If applied to the same set of anomalies from which the EOFs and PCs are computed, the result of such an operation is a pattern proportional to the EOF itself (apart from small differences induced by sampling problems). When model simulations are considered, one should not expect the composite anomaly to have the same amplitude as the analysis counterpart, since this would imply a perfect predictability of such a PC. However, if the projections on different EOFs were uncorrelated in the model, as they are in the analyses, the modelled composite anomaly should still be proportional to the analysed one, scaled by the correlation coefficient between observed and modelled PCs. If this is not the case, and a significant component of the model composite is orthogonal to the analysis composite, then flow-dependent model errors are likely to be responsible for the difference. Composites of 500 hPa height, 200 hPa divergence, and precipitation are compared in section 5(a).

(d) *Dynamical indices of planetary-wave forcing and propagation*

In addition to the listed fields, we also look at some dynamical quantities that are useful in understanding the response of the model to SST anomalies: The barotropic version of the generalized Eliassen–Palm (E–P) fluxes defined by Plumb (1985), and the refraction index for planetary waves.

The generalized E–P flux for stationary waves was suggested by Plumb (1985) as an extension to the three-dimensional (3-D) atmosphere of the original zonally averaged E–P fluxes (e.g. Andrews and McIntyre 1976). Here we use an approximation of the fluxes to a barotropic atmosphere, applied to the 200 hPa flow, assuming that the extra-tropical planetary waves we are interested in are mostly barotropic in their nature. The definition

of this flux is the following:

$$F_x = p \cos \phi \left(v'^2 - \frac{1}{2\Omega a \sin 2\phi} \frac{\partial(v'\Phi')}{\partial \lambda} \right) \quad (1)$$

$$F_y = p \cos \phi \left(-u'v' + \frac{1}{2\Omega a \sin 2\phi} \frac{\partial(u'\Phi')}{\partial \lambda} \right) \quad (2)$$

where F_x and F_y are the two horizontal components of the E-P flux, and all other symbols have their usual meteorological meaning, with primed variables representing eddy fields. A detailed derivation of these equations can be found in Plumb (1985).

The barotropic refraction index has been widely used in many studies on the propagation of planetary waves in the extra tropics, as in Hoskins and Karoly (1981) and Held (1983). It can be defined as the value of the critical wave number which separates the meridionally confined waves from those with a propagating structure profile. As such, the presence of relative maxima and minima in its latitudinal profile gives an indication of the possible confinement of planetary waves to mid latitudes.

In non-dimensional form, the index is defined as

$$K_c = \cos \phi \sqrt{\frac{a}{\bar{u}} \frac{\partial \bar{q}}{\partial \phi}} \quad (3)$$

where \bar{q} is the zonal-mean absolute vorticity and \bar{u} is the zonal-mean westerly wind. All waves characterized by a wave number smaller than K_c are able to propagate meridionally.

It should be pointed out that all these dynamical indices (and particularly the refraction index) have a strong nonlinear component. Therefore, when averaging these quantities among different ensemble members or different months, the dynamical indices are first computed from individual monthly means and then averaged, rather than being computed from composite wind and vorticity fields.

3. THE PATTERNS OF EURO-ATLANTIC EMPIRICAL ORTHOGONAL FUNCTIONS

This section describes the results of the EOF analysis of Euro-Atlantic 500-hPa geopotential-height anomalies from the NCEP dataset. In Fig. 1 we show the patterns of the four leading EOFs, scaled by the associated standard deviations. The patterns are computed as covariances between the 500 hPa geopotential-height anomalies and the standardized PCs; in this way, the connections with anomalies in other parts of the northern hemisphere can also be evaluated. These four EOFs explain 31%, 17%, 12% and 10% of the total variance respectively.

EOF1 (Fig. 1(a)) is representative of the NAO pattern (see Barnston and Livezey (1987), for an NAO definition based on mid-tropospheric height). A measure of consistency with the more usual NAO definition based on mean sea-level pressure (m.s.l.p.) is given by the correlation between the first PC and the time series of the m.s.l.p. difference between locations in Iceland and the Azores (e.g. Hurrell and van Loon 1997); such a correlation is 0.84 for the monthly means in our dataset.

EOF2 (Fig. 1(b)) has a strong similarity to the 500 hPa height eastern Atlantic pattern described by Wallace and Gutzler (1981). However, the anomalies associated with this EOF extend well beyond the Atlantic region; the hemispheric pattern resembles two clusters (namely, clusters no. 2 and 5a of the wintertime circulation defined by Molteni *et al.* (1990)).

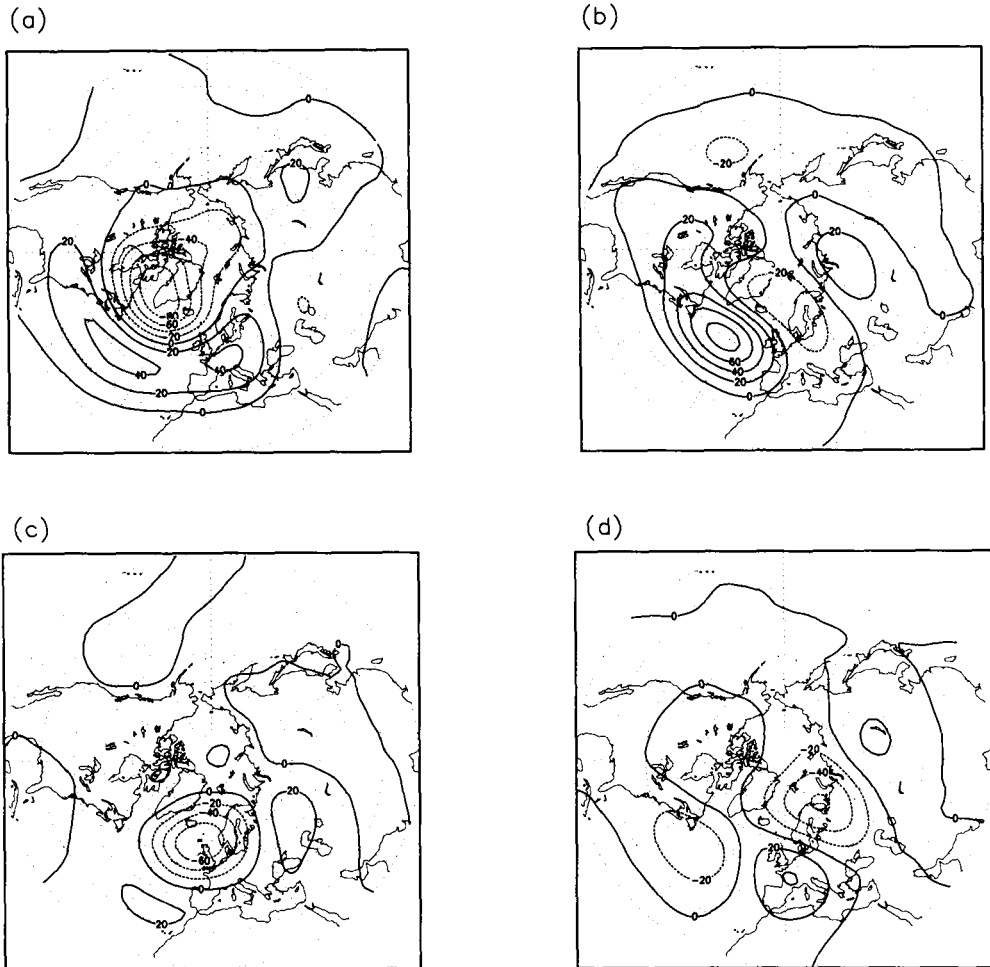


Figure 1. Patterns of the first four Euro-Atlantic empirical orthogonal functions (EOF1, EOF2, EOF3, EOF4) of 500 hPa height in winter (December–March) from National Meteorological Center/National Centers for Environmental Prediction analyses, computed as covariances between standardized principal components and monthly mean height anomalies. (a) EOF1, (b) EOF2, (c) EOF3, and (d) EOF4. Contour interval 15 m, negative contours dashed.

EOF3 (Fig. 1(c)) is clearly the most spatially confined of the four patterns in Fig. 1. In its negative phase, it bears a strong resemblance to the composite maps of Euro-Atlantic blocking shown by Tibaldi and Molteni (1990) and Tibaldi *et al.* (1994). Its strong association with blocking will be briefly discussed below, and explored in more detail in Pavan *et al.* (2000).

EOF4 (Fig. 1(d)) is similar to the Eurasian type-1 pattern of Barnston and Livezey (1987), and also shares some features with either the Southern Europe–North Atlantic (SENA) or the Scandinavian (SCAN) patterns defined by Rogers (1990) by a rotated PC analysis of m.s.l.p. monthly means. The correlation patterns extend over Siberia and North America. Its positive phase is characterized by increased zonal winds over the north-eastern Atlantic, Scandinavia and most of Siberia; the negative phase resembles a blocking dipole with centres over Scandinavia and France, with an opposite dipole over the western Atlantic.

TABLE 1. CORRELATION BETWEEN THE FIRST FOUR EMPIRICAL ORTHOGONAL FUNCTIONS (EOF1, EOF2, EOF3, AND EOF4) OF THE FULL DATASET (ROWS) AND THE EOFs COMPUTED RETAINING EVERY SECOND YEAR (COLUMNS)

	EOF1	EOF2	EOF3	EOF4
EOF1	0.98	0.04	-0.0001	0.14
EOF2	-0.04	0.97	-0.19	-0.08
EOF3	0.01	0.18	0.93	-0.30
EOF4	-0.15	0.08	0.22	0.95

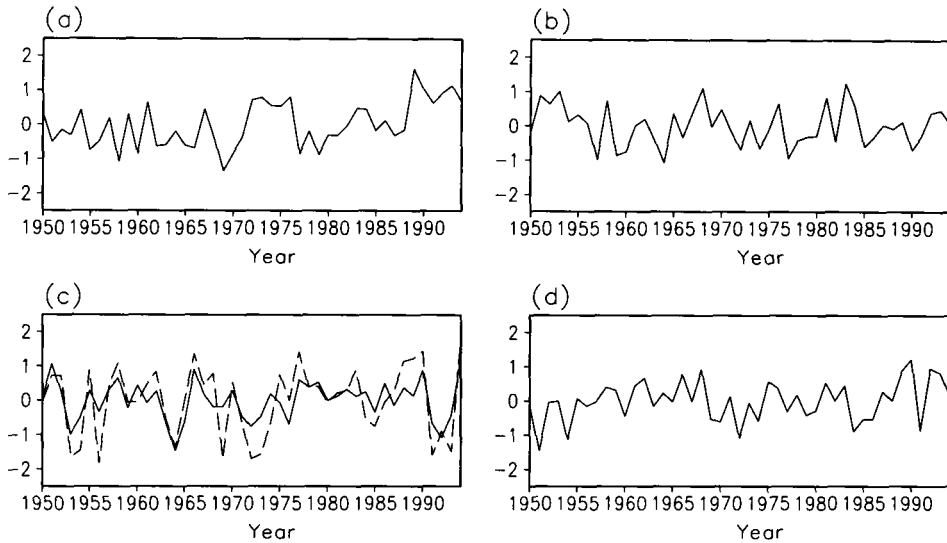


Figure 2. Time series of seasonal-mean values of: (a) the first principal component (PC), (b) the second PC, (c) the third PC and (opposite of) European blocking index, and (d) the fourth PC.

The stability of these EOFs was tested by recomputing them on various sub-samples, and by checking their sensitivity to the definition of the area boundaries. Their patterns were clearly reproduced in all tests whenever the chosen sub-sample of data spanned the full period of the original set. When shorter periods were considered, the presence of time trends (see below) produced some alterations of the statistical properties in the study. Table 1 shows the spatial correlations between the first four EOFs of the whole dataset and those obtained from a sub-sample of data including every second year only. The highest correlations are found between EOFs of the same rank. All other values are negligible, apart from the cross correlations with EOF3, which were found to be the least stable in all sub-samples.

Time series of the (seasonally averaged) values of the PCs (PC1, PC2, PC3, and PC4) associated with the four EOFs described above are plotted in Fig. 2. Figure 2(a) shows a clear upward trend in the values of PC1 during the last 20 years, which agrees with the NAO trend reported by various authors (e.g. Hurrell 1996; Hurrell and van Loon 1997; Zorita and Frankignoul 1997). No significant trend is evident for the other PCs.

Superimposed on the time series of PC3, Fig. 2(c) shows (the opposite of) a standardized index of the seasonal frequency of European blocking, obtained by computing

blocking frequency as a function of longitude according to the algorithm by Tibaldi and Molteni (1990), and then averaging the obtained frequency between 10°W and 50°E. Consistently with the structure of the EOF3 pattern, the anti-correlation between PC3 and the blocking-frequency index is quite strong (-0.76). One may note the persistence of positive values of PC3 during the period 1975–90, which is indicative of a decrease in the occurrence of blocks over western Europe.

4. RELATIONS BETWEEN EMPIRICAL ORTHOGONAL FUNCTIONS AND SEA SURFACE TEMPERATURES

We want now to investigate the link between the atmospheric large-scale flow patterns described by the four leading Euro–Atlantic EOFs and observed SST anomalies. The purpose of this analysis is to provide an observational basis for the interpretation of the results of the SST-forced ensemble integration. (The reader is referred to Wallace *et al.* (1992) and Deser and Timlin (1997) for a more comprehensive statistical analysis of the correlation between SST and height anomalies.) Here, we apply some basic statistical techniques to test whether some dynamical predictability of the EOF patterns may arise from SST forcing (and, if this is the case, where the forcing signal is coming from), or vice versa if the atmospheric anomalies described by the EOFs may cause significant variations in the underlying ocean temperature through anomalous energy fluxes.

Figure 3 shows the covariance maps of seasonally averaged SST from ERA against the corresponding values of the four standardized PCs, for the 14 winters covered by the ECMWF ensembles. These maps can be interpreted as the SST anomalies which correspond (through a linear relationship) to one standard deviation of the seasonal-mean PCs; the averages are computed from January, February and March (JFM) values, for consistency with the ensemble verifications discussed in section 5. The contours of the 14-winter climatology are also plotted as a reference. Given the limited length of the time series, one cannot attach a high statistical significance to these covariance maps. Still, a number of interesting features can be seen.

Looking first at the tropical Pacific (the main oceanic forcing region for the atmospheric circulation on a global scale), Figs. 3(b) and 3(d) show that the positive phases of EOF2 and EOF4 are associated with positive (i.e. El Niño-like) anomalies in the eastern Pacific in the region of the equatorial cold tongue, while an opposite anomaly is associated with the positive phase of EOF3 (Fig. 3(c)). No relevant features characterize the covariance with EOF1 (Fig. 3(a)) in this region.

The SST anomaly associated with EOF2 is clearly the largest in the eastern Pacific. In the western Pacific, however, the covariance anomaly for EOF4 shows a stronger meridional gradient between the equatorial and the sub-tropical region than the EOF2 anomaly. In section 5(b), it will be shown that this gradient has a noticeable impact on the intensity of the local Hadley circulation, as revealed by the structure of divergence and precipitation anomalies associated with the two EOF patterns.

For the SST anomaly associated with EOF3, the covariance map implies that blocking-like anomalies in western Europe (negative EOF3) occurred more frequently during El Niño winters than in other winters during the 1980–93 period. So far there is little support in the literature for a dynamical link between the two processes, which, in fact, is not supported by the analysis of the NCEP dataset in previous decades (see below).

It was mentioned above that, although seasonal means are normally used in studies of the relationship between SST and circulation anomalies, seasonal-mean results may mask differences in the response patterns which (in a linear framework) are

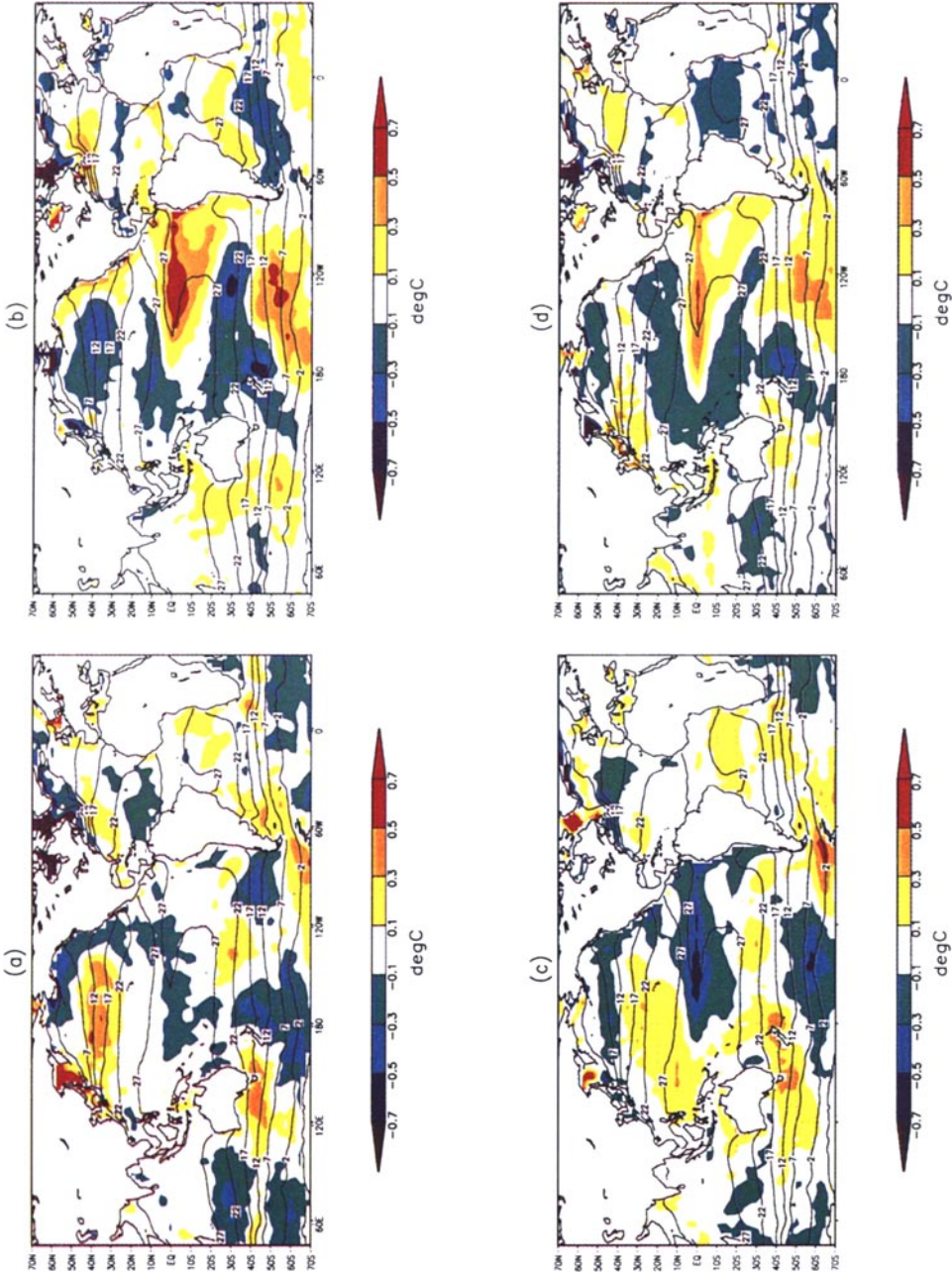


Figure 3. Covariances of European Centre for Medium-Range Weather Forecasts re-analysis (ERA) sea surface temperatures (SSTs) with (a) the first principal component (PC), (b) the second PC, (c) the third PC, and (d) the fourth PC. Contour interval 0.2 degC. The solid black contours show the ERA SST climatology with a contour interval of 5 degC.

TABLE 2. CORRELATIONS BETWEEN EMPIRICAL ORTHOGONAL FUNCTIONS AND EL NIÑO INDICES

	PC1	PC2	PC3	PC4
ERA JFM 80–93	−0.12	0.44	−0.42	0.33
NCEP JFM 65–79	−0.53	0.20	0.24	0.06
NCEP JFM 50–64	−0.20	0.20	−0.02	0.27
NCEP JFM 50–92	−0.20	0.28	−0.05	0.18
ERA JF 80–93	−0.05	0.16	−0.36	0.35
NCEP JF 50–92	−0.17	0.14	−0.06	0.19

PC1, PC2, PC3 and PC4 are the principal components associated with the first four empirical orthogonal functions. ERA is the ECMWF (European Centre for Medium-Range Weather Forecasts) re-analysis, and NCEP is the National Centers for Climate Prediction. JFM stands for January, February and March.

due to the seasonal changes in the basic-state circulation (e.g. Peng *et al.* 1995). It could be argued, for example, that the northern-hemisphere circulation in March already shows a weakening of the large-scale zonal asymmetries which characterize the climatological flow in the previous two months. When the covariances shown in Fig. 3 were recomputed using averages for January and February (JF) only, the results (not shown) revealed a reversal in the relative strength of the signal in the El Niño area between EOF2 and EOF4, the latter showing a larger covariance. The significance of these changes may be questioned, given the limited size of the ERA dataset; however, we show below that a similar result can be found in the longer record (1950 to 1992) provided by the NCEP SST dataset.

The NCEP reconstructed SSTs data (Smith *et al.* 1996) exhibit small differences from the ERA SSTs during the overlapping period, i.e. 1980 through 1992. (As discussed in section 2, the ERA SST mainly come from the dataset described by Reynolds and Smith (1994).) In particular, the seasonal covariances between SST anomalies and the first four PCs are almost identical to those shown in Fig. 3. Repeating the same analysis using all data available in the NCEP dataset, however, produces some significant differences, with a general decrease in the amplitude of the signal in the Pacific. This may be due to various causes, e.g. sampling problems in the ERA dataset, real interdecadal variability and/or differences in the data-analysis methods.

For brevity, we summarize the main results from the NCEP analysis in the Pacific region by comparing, in Table 2, the correlations between seasonal-mean values of PCs 1 to 4 and an ‘El Niño index’, obtained as the normalized time series of mean SST in the eastern equatorial Pacific (180°–90°W, 5°S–5°N). (This region covers the so-called Niño-3 area, but its longitudinal extent is 30° wider; the reason for this extension is a greater stability of the correlations discussed below.)

As a reference, the first row of Table 2 shows the correlation obtained using seasonal means of PCs and ERA SSTs in the JFM period. Consistently with the covariance maps in Fig. 3, the largest absolute correlation is obtained for PC2, the smallest absolute value for PC1. The second and third row of the table show the corresponding JFM correlations obtained from the NCEP dataset in two preceding 15-year periods, namely 1965–79 and 1950–64. For PC2 and PC4, the correlations keep the same (positive) sign as in the ERA period, although with reduced amplitude. The negative correlation between PC1 (our NAO index) and the El Niño index is also confirmed, but in this case the amplitude is stronger than in the ERA period (and notably so in 1965–79). On the other hand, the PC3 correlation ranges from negative (in the ERA period) to weakly positive or insignificant.

The fourth row of Table 2 summarizes the JFM correlations as obtained from the full NCEP dataset (1950–92). Apart from PC1, the relationship between the El Niño index and all other EOFs is reduced in the extended dataset. The NCEP results seem to exclude any relationship between El Niño and the blocking-like EOF3, and this will be confirmed by the ensemble diagnostics in the next section. On the other hand, a possible (weak) influence of El Niño on the NAO-like EOF1 cannot be totally ruled out on the basis of the NCEP data. With regard to the association with EOF2 and EOF4, decadal trends in the large-scale circulation patterns (e.g. Corti *et al.* 1999) might have created dynamical conditions more favourable to the manifestation of an El Niño response along these two patterns in the ERA period.

In this respect, it is interesting to re-examine the issue of the sensitivity to seasonal changes to the basic state using the full NCEP record. The last two rows of Table 2 compare the correlations for the ERA and the total NCEP record using JF averages. The difference between the ERA and NCEP values obviously reflects the JFM results, but it is interesting that in both datasets the JF-only correlation of PC2 with El Niño is strongly reduced with respect to the JFM value. The marked seasonality in the EOF2 response suggests that the predictability of this pattern as a response to boundary forcing may be strongly affected by changes in the structure of the time-mean flow (see also section 6).

Finally, in exploring the relationship between the Euro–Atlantic circulation patterns and Pacific SSTs, one should not neglect the existence of possible correlations outside the El Niño region. The covariances in the west Pacific associated with PC4 were already mentioned in the discussion of Fig. 3. Indeed, in the ERA period, the JFM-mean PC4 shows a correlation of -0.53 with SSTs averaged in a western equatorial Pacific region (120° – 160° E, 5° S– 10° N), and of 0.50 with SST in the mid-latitude west Pacific (120° – 160° E, 30° – 45° N), both stronger (in absolute value) than the El Niño correlation. The importance of the signal in the west Pacific region for the predictability of PC4 will be supported by the results shown in the next section.

Now we turn to the relationship between the leading EOFs and SST anomalies in the Atlantic ocean. Specifically, we want to investigate whether such an association should be interpreted as the result of anomalous forcing of the atmospheric circulation by SST anomalies (as modelled by Palmer and Sun (1985)), or rather as having been caused by atmospheric anomalies affecting the ocean through anomalous heat fluxes (e.g. Cayan 1992; Battisti *et al.* 1995).

A simple way to discriminate between the two hypotheses is to compute lag correlations between atmospheric and oceanic indices (as in Wallace and Jiang 1987; Deser and Timlin 1997), and check whether the largest correlations are obtained at lag 0 (as expected in the case of SST forcing the overlying atmosphere) or for oceanic variables lagging the atmospheric ones. We, therefore, computed month-by-month lagged correlation between PCs and SSTs. Consistently with previous studies performed on monthly means, we found that north of 20° N there is a strong temporal asymmetry in the lag correlations: The maps at ocean lag 1 show slightly larger correlations than those at lag 0, while those at lag -1 have a much weaker signal. Overall, these correlations (which are not shown for brevity) suggest that the SST anomalies in the North Atlantic are largely due to the influence of atmospheric anomalies on the upper ocean, confirming earlier results by Cayan (1992), Battisti *et al.* (1995), and Zorita and Frankignoul (1997) among others.

Despite the evidence of the forcing of SST by extra-tropical atmospheric anomalies, the question of the existence of a positive feedback of extra-tropical SST onto the atmospheric flow is crucial for the understanding of ocean–atmosphere variability on both interannual and interdecadal time-scales. The success obtained recently by Rodwell

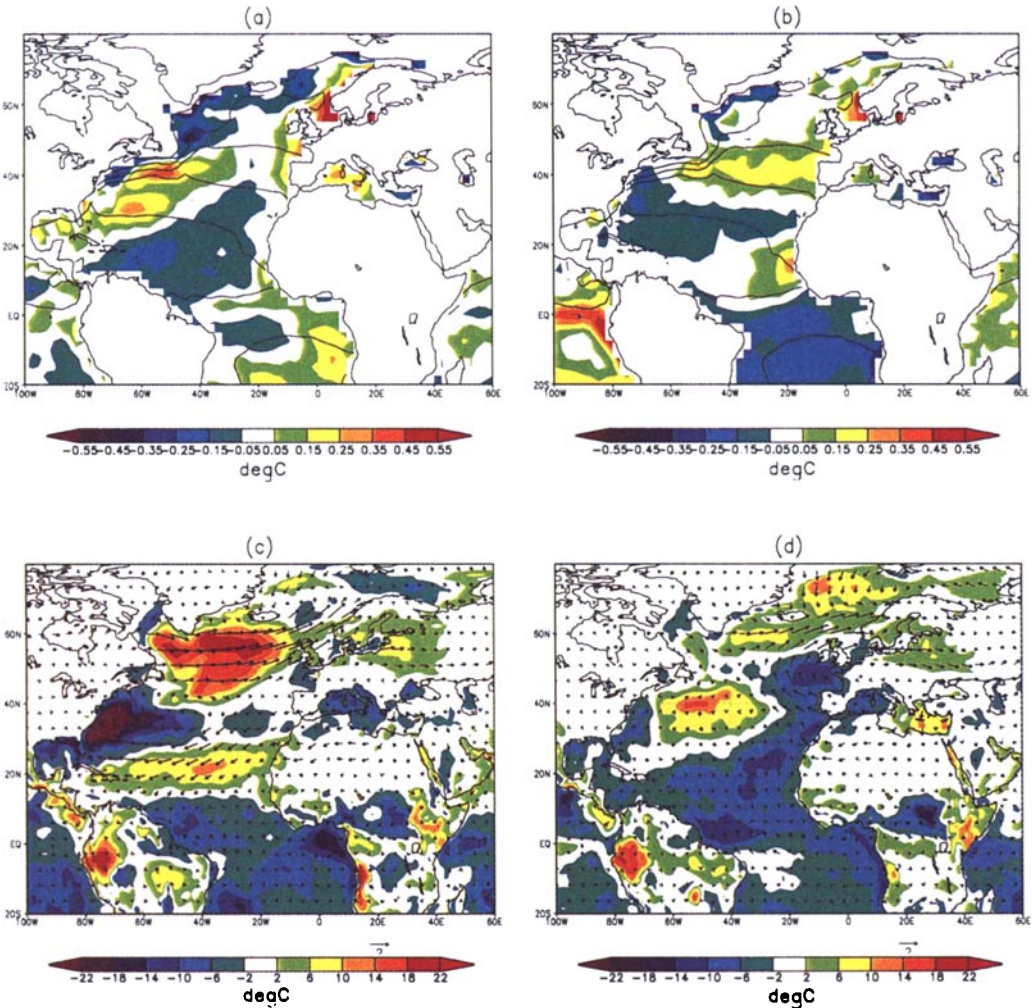


Figure 4. Top panels: Covariances of European Centre for Medium-Range Weather Forecasts re-analysis (ERA) sea surface temperatures (SSTs) with (a) the first principal component (PC1) and (b) the fourth principal component (PC4). Contour interval 0.1 degC. The solid black contours show the ERA SST climatology with a contour interval of 5 degC. Bottom panels: Covariances of ERA latent-heat flux and 10 m wind with (c) PC1, and (d) PC4. Contour interval 4 W m^{-2} .

et al. (1999) in simulating the decadal variability of the NAO index in an ensemble simulation forced by observed SSTs is strongly supportive of the positive feedback hypothesis. However, to what extent the physical and dynamical interactions occurring in SST-forced experiments are representative of the interactions in a coupled system remains an open question. Commenting on results of experiments with an idealized North Atlantic SST anomaly, Rodwell *et al.* noted that the simulated latent-heat flux (LHF) anomalies were in phase with the SST anomalies (see their Figs. 3(a) and 3(c)), which contradicts the existence of a positive feedback of evaporation on SST claimed by previous authors (Latif and Barnett 1994; Grotzner *et al.* 1998).

In Fig. 4 we compare the covariance of ERA SST with PC1 and PC4 over the North Atlantic region with the covariance of the same PCs with ERA near-surface winds and LHF. In the case of PC1, it is evident that the ERA LHF anomalies are

TABLE 3. STATISTICAL EVALUATION OF THE ECMWF ENSEMBLE EXPERIMENTS

	EOF1	EOF2	EOF3	EOF4
σ_{obs}	0.76	0.71	0.56	0.69
σ_{ens}	0.62	0.61	0.66	0.80
$\sigma_{\overline{\text{ens}}}$	0.39	0.33	0.33	0.35
$\sigma_{\overline{\text{ens}}}/\sigma_{\text{ens}}$	0.63	0.54	0.50	0.44
$\overline{\text{ens}} - \text{obs}$	0.13	-0.45	1.24	0.50
$\text{corr}_{\text{obs};\overline{\text{ens}}}$	0.33	0.004	0.10	0.69

See text for further explanation.

markedly out of phase with the SST anomalies north of 10°N, and that they are, rather, determined by variations in surface wind. So, LHF anomalies are positive wherever the surface-wind anomalies reinforce the winter-mean flow, and negative where the wind anomalies decrease the total-wind amplitude. This behaviour is consistent with the lag correlations, and (in a coupled system) would imply a positive feedback onto the NAO pattern associated with evaporation. For PC4, on the other hand, the anti-correlation between SST and LHF anomalies is limited to the eastern side of the North Atlantic, where circulation anomalies are stronger, while on the western half of the ocean SST and LHF tend to be in phase because of the absence of significant wind anomalies. In the tropical Atlantic, the LHF covariance with PC4 shows a strong negative anomaly which is mostly in phase with the SST pattern. The SST and LHF covariances associated with PC2 and PC3 (not shown) tend to show relationships similar to those displayed by PC1 and PC4 (respectively) in the extra tropics, with weaker signals in the tropical Atlantic.

5. VALIDATION OF THE WINTER ENSEMBLE INTEGRATIONS

In this section, the winter ensemble forecasts described in section 2(c) are validated against fields from ERA. Time series of PCs and composite anomalies are used to verify to what extent the ensembles reproduce anomalies associated with the four leading EOFs of 500 hPa height described in the previous sections.

(a) Time series of principal components

Figure 5 shows the projections of the seasonal (JFM) average 500 hPa height anomalies on the four EOFs for both ERA and the ensemble integrations, normalized using the 45-winter standard deviation of monthly mean values. (In this way, the ERA projections are practically identical to the original PC values for the same period.) Table 3 (rows 1 to 3) lists the standard deviations of various quantities shown in Fig. 5, namely the ERA time series (σ_{obs}), the whole set of ensemble realizations (σ_{ens}) and the ensemble-mean time series ($\sigma_{\overline{\text{ens}}}$). Rows 4 and 5 of Table 3 show the bias between the ensemble-mean and ERA data ($\overline{\text{ens}} - \text{obs}$) and the correlation coefficients between these two time series ($\text{corr}_{\text{obs};\overline{\text{ens}}}$).

By squaring the σ_{obs} values, one finds that the seasonal (JFM) average of the first PC explains about 60% of the monthly mean variance; this fraction is reduced to about 50% for PC2 and PC4, and to little more than 30% for PC3. Consistently with the results of section 4, among the four EOFs considered EOF3 appears the least likely to be influenced by a slowly varying boundary forcing.

Comparing observed and modelled values, a large systematic shift of the model projections toward more positive values is evident in the case of EOF4 (Fig. 5(d)) and especially of EOF3 (Fig. 5(c)). Since both EOFs are associated with blocking in their

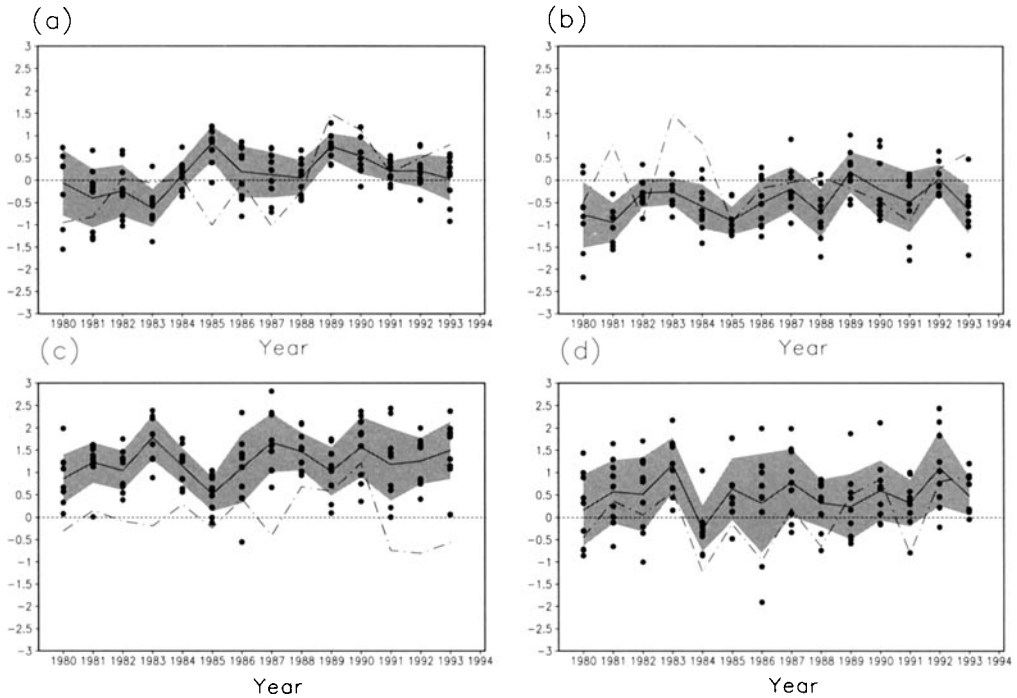


Figure 5. Projection of January/February/March (JFM) average anomalies of 500 hPa height on (a) the first empirical orthogonal function (EOF), (b) the second EOF, (c) the third EOF, and (d) the fourth EOF from the individual ensemble experiment (dots) and their ensemble mean (solid line). The shaded strip indicates the interval of one standard deviation around the mean of each ensemble. The dash-dotted line shows the projection of the JFM 500 hPa height anomalies from the European Centre for Medium-Range Weather Forecasts re-analysis on the EOFs.

negative phase, such a result indicates an inability of the ECMWF model to simulate an adequate number of blocks over Europe. This deficiency has been documented for earlier versions of the ECMWF model (Ferranti *et al.* 1994a,b; Branković and Molteni 1997), and does not appear to have been overcome yet.

As far as the variance distribution is concerned, the magnitude of the σ_{ens} term is comparable to the observed values, but the differences in variance between various EOFs are poorly simulated. The model overestimates the variability of EOF3 and EOF4, which explain more variance than EOF1 and EOF2 in the individual integrations. In the previous section, it was noted that the relationship between heat fluxes and SST anomalies in the North Atlantic was not the same for all EOFs according to ERA data. For EOF1 and EOF2, the heat-flux anomalies were mainly wind driven, and were anti-correlated with SST anomalies. By creating a positive feedback on SST, the heat fluxes should enhance the variability of the coupled ocean-atmosphere system with respect to a forced system with prescribed SST. The opposite should occur when heat-flux and SST anomalies are in phase, as occurred in the composites associated with EOF3 and EOF4 (at least in the western half of the North Atlantic). So the distribution of the EOF total variance in the ECMWF ensembles is consistent with the absence of a feedback of the atmospheric circulation on the extra-tropical ocean.

On the other hand, by filtering out most of the variability generated by internal atmospheric dynamics, ensemble means should emphasize the forced component of the atmospheric circulation. Looking at the standard deviations of ensemble means ($\sigma_{\overline{\text{ens}}}$),

EOF1, interestingly, regains its leading role. Assuming the ratio between ($\sigma_{\overline{\text{ens}}}$) and σ_{ens} is a measure of predictability, one finds that this ratio decreases monotonically from 63% for EOF1 to 44% for EOF4.

In a perfect-model environment, in which the statistical properties of individual ensemble members (e.g. their means and variances) are assumed to be equal to their observed counterparts, one should find a proportionality (within sampling errors) between this ratio and the correlation between ensemble means and observed values. In reality, one finds a modest correlation for EOF1 (33%, significant at the 85% confidence level), practically no correlation for EOF2 and EOF3, and a 69% correlation (significant at the 99% level) for EOF4, which is clearly noticeable from the time series in Fig. 5(d). Therefore, predictability estimates from modelled data should be taken cautiously (not necessarily in a negative sense, as the case of EOF4 shows) in the presence of significant systematic model errors (cf. $\overline{\text{ens}} - \text{obs}$ in Table 3).

A closer inspection of the time series in Fig. 5 gives some further insight into the model behaviour. As far as EOF1 is concerned, the positive correlation between ensemble means and observed data seems to come more from the decadal positive trend in the NAO index than from year-to-year variations. The lowest ensemble-mean value is obtained in JFM 1983 (El Niño event), the two highest values in 1985 and 1989 (La Niña events). However, among these three winters only in 1989 does one find a large observed anomaly with the same sign as the ensemble mean. So, the modelled interannual variations are somehow consistent with a weak inverse relationship between EOF1 and El Niño, which (according to Table 2) was more evident in the analysed record before 1979 than during the ERA period. Support for the hypothesis that decadal variations of the NAO index may be more reproducible (in simulations forced by observed SST) than its shorter-term variations comes from the ensemble simulations of Rodwell *et al.* (1999). They report that a correlation of 0.41 between the observed and simulated NAO index (based on surface pressure) rises to 0.74 when fluctuations with periods shorter than 6.5 years are filtered out.

For EOF2, the time series of the observed projections shows the largest value during the major El Niño event of winter 1982/83. The unusual strength of SST and atmospheric anomalies during that event may explain why the correlation between PC2 and the Niño-3 index during the ERA period is larger than in previous decades (see section 4). However, even accounting for interdecadal fluctuations in the correlation between PC2 and the El Niño index (shown in Table 2), the absence of any correlation between the observed and the ensemble-mean projections on EOF2 is still inconsistent with observations, and can hardly be justified by sampling problems. One should note that the observed projection in JFM 1983 is well outside the ensemble range, suggesting that the simulation of this EOF is affected by model errors.

With regard to the predictability of EOF4, it would be wrong to play down the importance of the good simulation of this EOF, simply because of the relatively low ranking of this pattern in the 45-winter sample of monthly means, or the smaller proportion of explained variance with respect to the NAO pattern (EOF1). Actually, a good deal of the EOF1 variance is explained in the Atlantic region, while over Europe the two patterns have a closer amplitude (see Fig. 1; in the following, it will also be shown that the associated rainfall anomalies over Europe are comparable). Moreover, neglecting the variance associated with interdecadal variability, the difference in variance between the two EOFs is reduced even further: The standard deviation of seasonal means in the 14-winter sample analysed here is only 10% lower for PC4 compared with PC1.

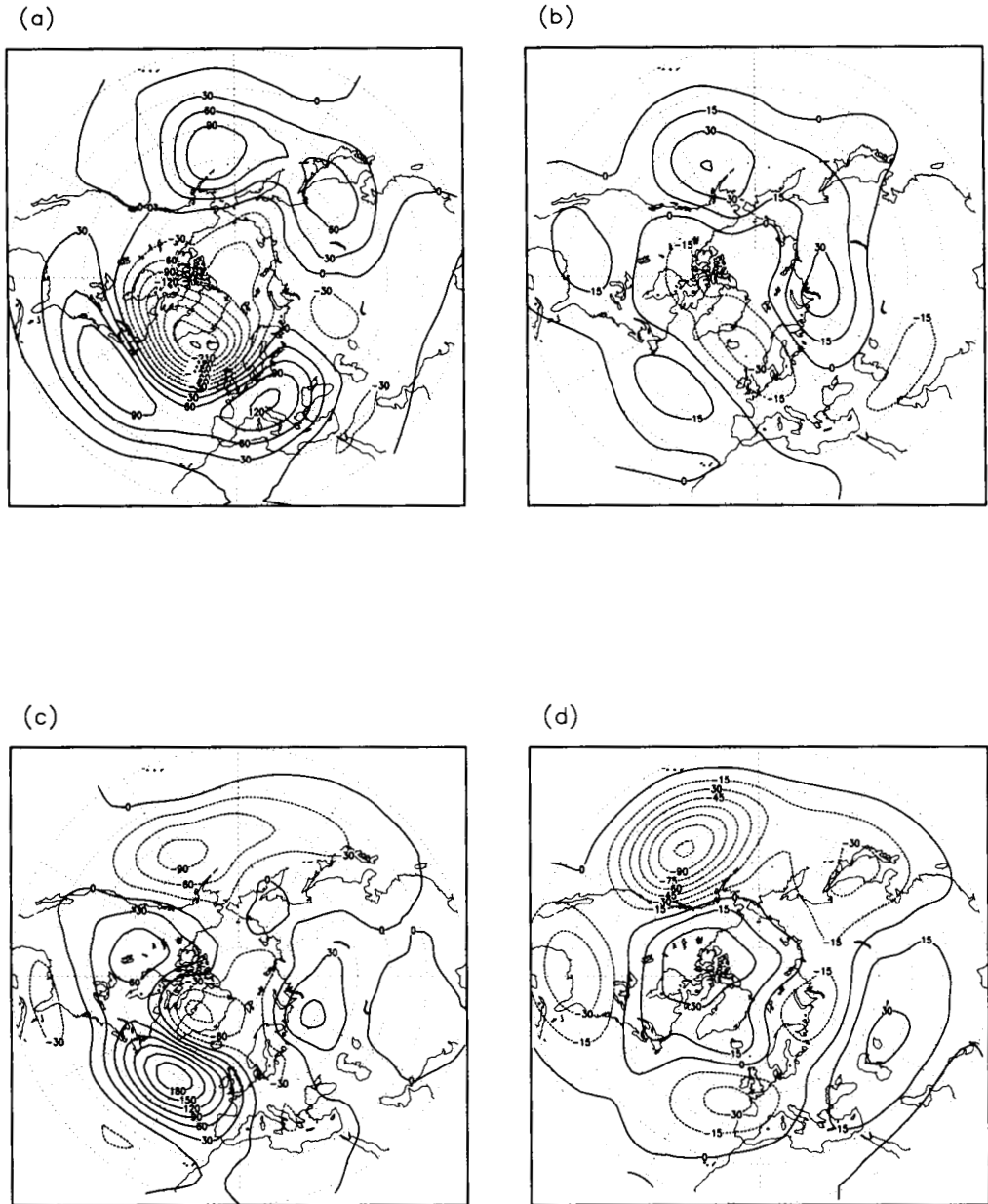


Figure 6. Composite anomalies of 500 hPa height from the European Centre for Medium-Range Weather Forecasts (ECMWF) re-analysis (ERA) (left panels) and ECMWF ensembles (right panels) associated with the first empirical orthogonal function (EOF) ((a) and (b)), the second EOF ((c) and (d)), the third EOF ((e) and (f)), and the fourth EOF ((g) and (h)). Each composite is a difference between the mean anomaly of those months in which the standardized ERA principal component (PC) of the ERA anomaly is greater than 0.67 and the mean anomaly of months when the ERA PC is less than -0.67 . (a), (c), (e), and (g) ERA composites, contour interval 30 m; (b), (d), (f), and (h) ensemble composites, contour interval 15 m.

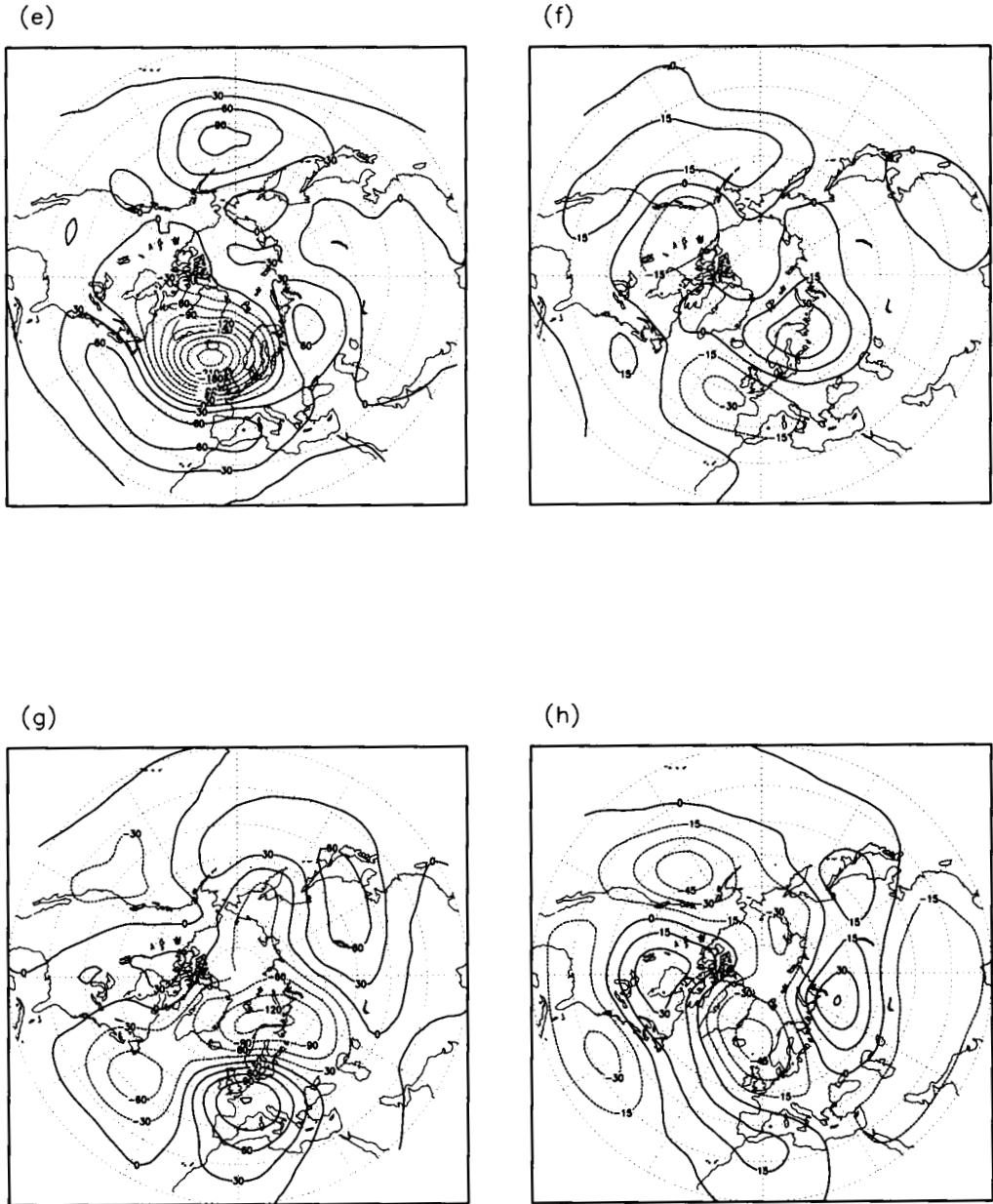


Figure 6. Continued.

Finally, we point out that, in the ERA period, the observed response to El Niño events in the Euro-Atlantic sector does not show a recurrent spatial pattern, as it does in the PNA area. Considering the three warm events of 1983, 1987, and 1992; in the first winter the observed anomaly has a large projection on EOF2, in the second winter EOF1 has the largest signal, while in 1992 the projections on EOF3 and EOF4 are the strongest ones.

TABLE 4. SPATIAL CORRELATION BETWEEN THE EUROPEAN CENTRE FOR MEDIUM-RANGE WEATHER FORECASTS RE-ANALYSIS DATA AND MODEL COMPOSITES OF 500 hPa height

EOF1	EOF2	EOF3	EOF4
0.54	-0.28	0.04	0.23

EOF1, EOF2, EOF3, and EOF4 are the first four empirical orthogonal functions.

(b) *Anomaly composites*

We now compare composite anomalies from ERA and model fields, constructed by using the observed standardized PCs of 500 hPa height as a reference (see section 2(c) for details). The purpose of this analysis is to highlight flow-dependent errors in the model simulations, which may cause differences between the spatial patterns of observed and modelled composites. (A difference in amplitude may arise from the limited predictability of the observed anomalies, even in a perfect-model environment.)

Each composite is computed as a difference between the average anomaly in those months when the standardized PC of the ERA 500 hPa height anomaly is larger than 0.67, and the average anomaly in those months when the same quantity is smaller than -0.67. The threshold of 0.67 has been chosen because, in the case of a normalized Gaussian distribution, the total frequency of values larger than 0.67 or smaller than -0.67 is equal to 50%. This should guarantee that, even with just a 14-winter sample, the number of monthly anomalies falling in each composite is large enough to generate fairly reliable statistics. When plotting such composites, the contour interval chosen for the ERA fields may be larger than the one chosen for the model fields, reflecting the (expected) amplitude reduction.

In Fig. 6, composites of 500 hPa height anomalies are shown for ERA and the model ensembles. In agreement with the results of the time-series analysis, we find that the composites for EOF2 and EOF3 show the strongest discrepancies between the model and the analysis. For EOF2 in particular, the model composites over Europe and the eastern Atlantic are almost completely out of phase with the analysis. Such a poor model response is quite remarkable when compared with the excellent agreement (even in amplitude) over the PNA region, which undoubtedly arises from the response to tropical SST anomalies (cf. Fig. 3(b)). The phase of the western-European dipole represented by EOF3 is also reversed in the ensemble simulations. The North Atlantic dipole associated with the NAO pattern (EOF1) has the correct phase, but over Europe the correspondence is poorer. This situation is somehow reversed for the EOF4 composites. The anomalies over western Europe are rather well represented by the model, together with the zonally oriented anomalies over Asia which are associated with strong zonal winds over Siberia in the positive phase of EOF4. On the other hand, over the western Atlantic Ocean and North America, the model EOF4 composite shows a weaker similarity to its observed counterpart.

One can quantify the agreement between the observed and modelled composites by computing the spatial correlation between the two patterns in the region of definition of the EOFs (20°–90°N, 90°W–60°E). These spatial correlations, listed in Table 4, again indicate EOF1 and EOF4 as the most predictable patterns, but in this case the best result is obtained for EOF1. This depends on the relatively good simulation of the NAO pattern

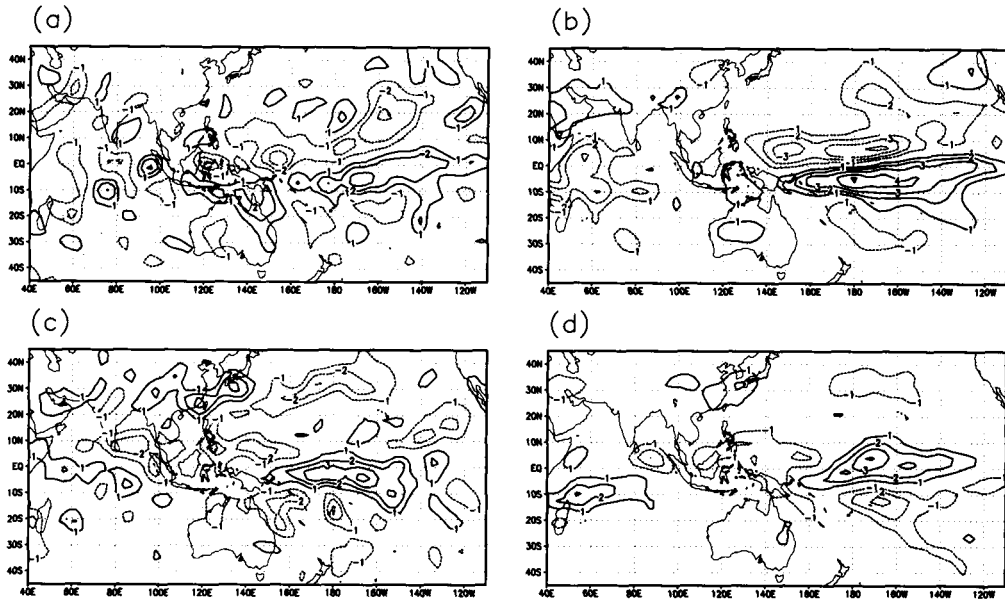


Figure 7. Composite anomalies of 200 hPa divergence computed for the second empirical orthogonal function (EOF) ((a) and (b)) and the fourth EOF ((c) and (d)). (a), and (c) the European Centre for Medium-Range Weather Forecasts re-analysis composites, (b) and (d) ensemble composites. Contour interval 10^{-6} s^{-1} , zero contour omitted. Composites are defined as in Fig. 6.

over the Atlantic Ocean; if the correlations were computed over the Eurasian continent, the ranking of EOF1 and EOF4 would be reversed.

In evaluating predictability induced by SST forcing, the potential influence of tropical SST anomalies is obviously of crucial importance. If the relationship between EOF2/EOF4 and tropical Pacific SST suggested by the ERA data reflected a real dynamical link (and therefore a potential predictability of these large-scale anomalies), an accurate simulation of fields closely related to tropical diabatic forcing (e.g. upper-troposphere divergence and precipitation) should be a prerequisite for a skilful seasonal prediction of these EOF patterns.

Figure 7 shows composites of analysed and simulated anomalies of 200 hPa divergence, in a tropical band covering the Indian and Pacific Oceans, for EOF2 and EOF4 (maps for EOF1 and EOF3 are not shown because a much weaker signal is present in the corresponding model composites for this field and area). Overall, the model simulations of divergence anomalies over the tropical Pacific are quite satisfactory, and show no reduction of amplitude with respect to the observed counterparts (they are even stronger than observed in the case of EOF2). If the spatial correlation of ERA and model composites is computed in the area (100°E – 120°W , 10°S – 10°N), one finds a larger value (0.65) for EOF4, compared with 0.30 for EOF2.

Over the Indian Ocean and the Pacific north of 20°N , the comparison is more difficult because of the noisiness of the observed field; however, a careful inspection again shows a better simulation for EOF4 than for EOF2. Note, in particular, the positive anomaly between east China and Japan, which is consistent with the positive SST anomaly in the western extra-tropical Pacific shown in Fig. 3(d), and is indicative (together with the negative anomaly over the maritime continents) of a reduction in the Hadley circulation over the western Pacific.

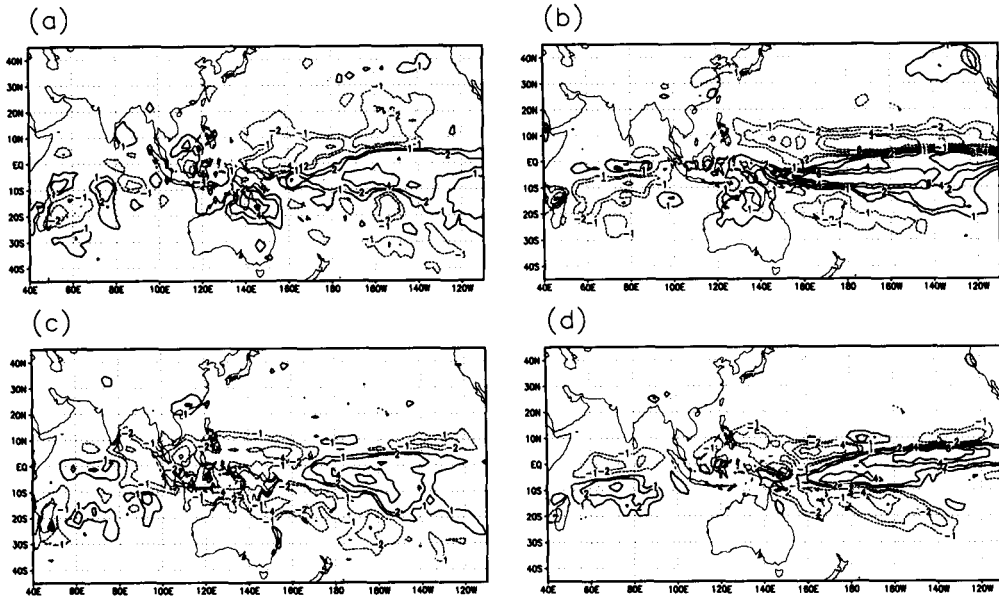


Figure 8. As Fig. 7, but for precipitation composites from Xie and Arkin (1996) data ((a) and (c)), and European Centre for Medium-Range Weather Forecasts ensembles ((b) and (d)). Contours at -6 , -4 , -2 , -1 , -0.5 , 0.5 , 1 , 2 , 4 and 6 mm day^{-1} . Composites are defined as in Fig. 6.

Figure 8 shows precipitation composites for the same region and EOFs displayed in Fig. 7. The observed anomalies are derived from the Xie and Arkin (1996) dataset. Again, the model simulations over the central tropical Pacific are definitely good, although they overestimate the amplitude of the rainfall anomalies. Interestingly, over the Indonesian region the largest (negative) observed anomalies are those associated with EOF4, which agrees with the negative correlation (-0.53) between observed values of PC4 and west Pacific SST reported earlier.

Commenting on Fig. 4 in the previous section, strong latent-heat-flux anomalies in the tropical Atlantic were noted in the ERA composites associated with EOF1 and EOF4. These are likely to be reflected in the rainfall distribution. Rainfall composites over the northern and tropical Atlantic for EOF1 and EOF4 are compared in Fig. 9. The observed composites show differences between the patterns of tropical Atlantic rainfall associated with these two EOFs. The tropical anomaly associated with EOF1 (NAO) has a dipole shape between 60°W and 20°W , with positive values north of the equator and negative values below. It should be noted that the positive rainfall anomaly over the tropical ocean occurs in a region of negative SST anomalies (see Fig. 4(a)), and is, therefore, due to the enhanced moisture convergence associated with the strengthening of the trade wind in the positive NAO phase (Fig. 4(c)). For EOF4, a negative anomaly straddles the equator from the Amazon basin to the Gulf of Guinea (consistent with the negative latent-heat-flux anomalies in Fig. 4(d)), while positive anomalies cover south Brazil and east Africa.

The model composites are more similar to each other than are the observed ones; both have a dipole structure similar to the observed EOF1 composite. Over Brazil, the simulated rainfall composite for EOF4 is almost out of phase with the observed counterpart. The better model performance in reproducing the pattern of tropical Atlantic rainfall for EOF1 than for EOF4 might be invoked as a (partial) explanation of the better

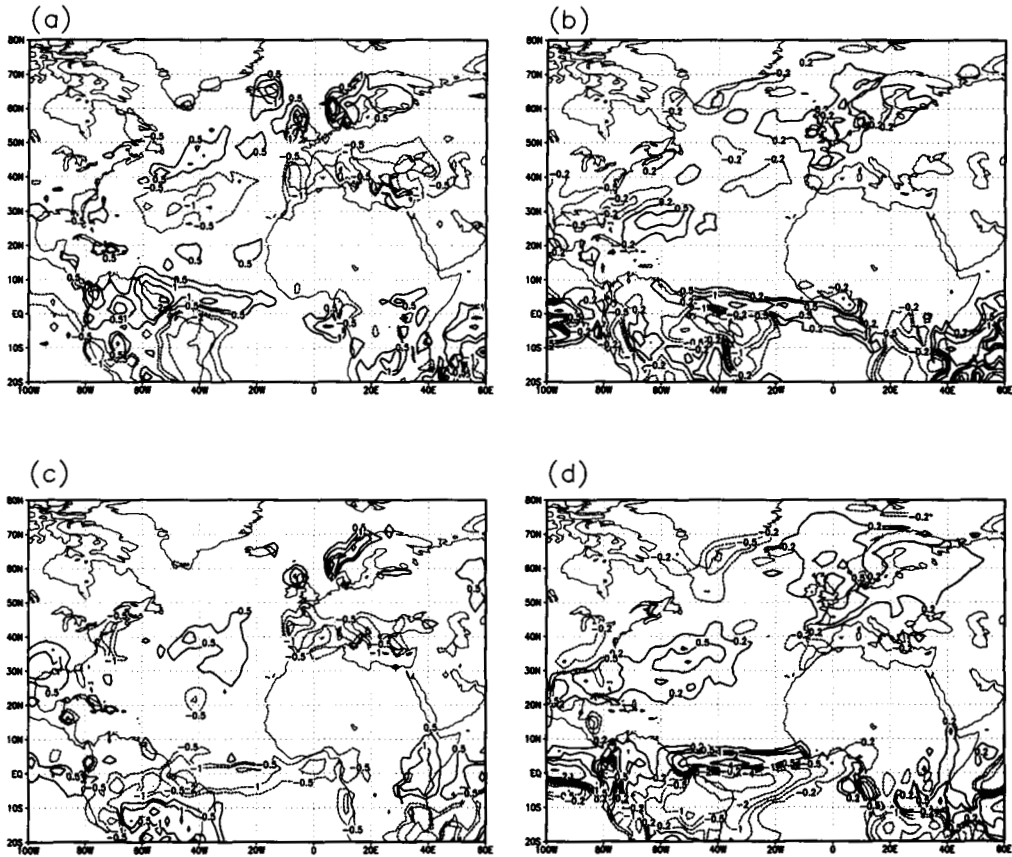


Figure 9. Precipitation composites in the Atlantic region associated with the first empirical orthogonal function (EOF) ((a) and (b)) and the fourth EOF ((c) and (d)). Panels (a) and (c) from Xie and Arkin (1996) data, contours at $-4, -2, -1, -0.5, 0.5, 1, 2, 4 \text{ mm day}^{-1}$; panels (b) and (d) from European Centre for Medium-Range Weather Forecasts ensembles, contours at $-4, -2, -1, -0.5, -0.2, 0.2, 0.5, 1, 2, 4 \text{ mm day}^{-1}$. Composites are defined as in Fig. 6.

spatial correspondence between observed and modelled circulation composites over the Atlantic (see the discussion on the 500 hPa height composites above). However, the strong role played by trade-wind anomalies in setting the moisture convergence pattern could actually justify an opposite cause-and-effect relationship.

In the extra tropics, both EOF1 and EOF4 (in their positive phase) are associated with increased rainfall over northern Europe and dry conditions over the Mediterranean. (The presence of a substantial correlation between the NAO and the winter precipitation over Europe during the last century has been documented by many authors: Rodó *et al.* (1997), Hurrell (1995), Valero *et al.* (1996) and Hurrell and van Loon (1997)). The model reproduces the northern European anomaly reasonably well, although it spreads it out over a much wider region. The Mediterranean dry anomaly, conversely, is hardly visible in the model composites. The poor resolution of European topography in the T63 model is likely to have a negative impact on the realism of the rainfall simulations in the region.

6. DISCUSSION AND DYNAMICAL INTERPRETATION

The results discussed in the previous sections have provided a rather complex picture of the predictability of Euro–Atlantic large-scale anomalies. It is evident that different dynamical mechanisms play a role in determining the Euro–Atlantic variability on monthly to seasonal time-scales, and that some of them are better simulated than others by the ECMWF model. This is reflected by the different predictability of the four leading EOFs analysed in this paper.

For EOF1, which represents the NAO pattern, the wintertime predictability estimated from the ECMWF ensembles (quantified by the correlation between ensemble-mean and re-analysis PCs) is comparable to corresponding estimates from multi-decadal simulations with the Hadley Centre GCM reported by Davies *et al.* (1997) and Rodwell *et al.* (1999). Although these studies have emphasized the importance of the ocean–atmosphere interactions for the interdecadal variability of the NAO, on the interannual time-scale the atmospheric internal dynamics are apparently the dominant source of variability, and the feedback of extra-tropical SSTs on the atmospheric circulation seems to account for a relatively small proportion of the NAO variance.

Are there Euro–Atlantic patterns which are influenced by ENSO-related anomalies, and through which mechanism? On this issue, the results of our investigation are partially contradictory. In the analysis, the strongest correlation between Euro–Atlantic PCs and tropical Pacific SSTs is found for EOF2, which resembles the eastern Atlantic pattern of Wallace and Gutzler (1981), but is also associated with significant anomalies in the Pacific region. This relationship is confirmed by the observed and model composites of rainfall and upper-tropospheric divergence associated with this pattern, which show a large and well simulated signal in the central tropical Pacific. The corresponding extra-tropical anomalies in the Pacific sector are well simulated in the geopotential composites. However, the Euro–Atlantic components of these composites are poorly represented in the model, and ensemble simulations of the associated PCs show no predictive skill.

Can one find some explanation for the poor simulation of EOF2 in the Euro–Atlantic sector, despite the fact that the associated signal in the east Pacific is so well captured? In section 4, the observed correlation between PC2 and the El Niño index was found to be sensitive to the phase of the seasonal cycle, being stronger in late winter than in early winter. Based on this result, we hypothesized that simulations of the EOF2 response might be strongly affected by the structure of the time-mean flow. Figure 10 compares the JFM systematic error of 200 hPa wind, computed from the 14-winter ensembles, with the climatological 200 hPa wind difference (March minus January), estimated from ERA. (This variable was chosen since planetary-wave propagation is known to be strongly affected by the distribution of upper-tropospheric zonal winds.) Over the tropical and north Pacific, the systematic error of the ECMWF model is strongly correlated with the March-minus-January difference. In the Pacific region, therefore, the model has a mean circulation more similar to observed flow in late winter, when the EOF2–El Niño correlation is stronger. In the North Atlantic region; vice versa, the two maps tend to be anti-correlated. For example, the area of positive (i.e. westerly) errors between 40°N and 60°N is mostly out of phase with the seasonal change. Features in the Caribbean region are similarly anti-correlated. In the Euro–Atlantic sector, therefore, the model circulation is more representative of early winter conditions, when the EOF2 pattern is less affected by Pacific SST according to the observed record.

On the other hand, a significant predictability is found for EOF4, which represents a zonal wave-number-2 pattern with important features over the Eurasian continent. This pattern is associated with variations of rainfall and divergence in the west Pacific and

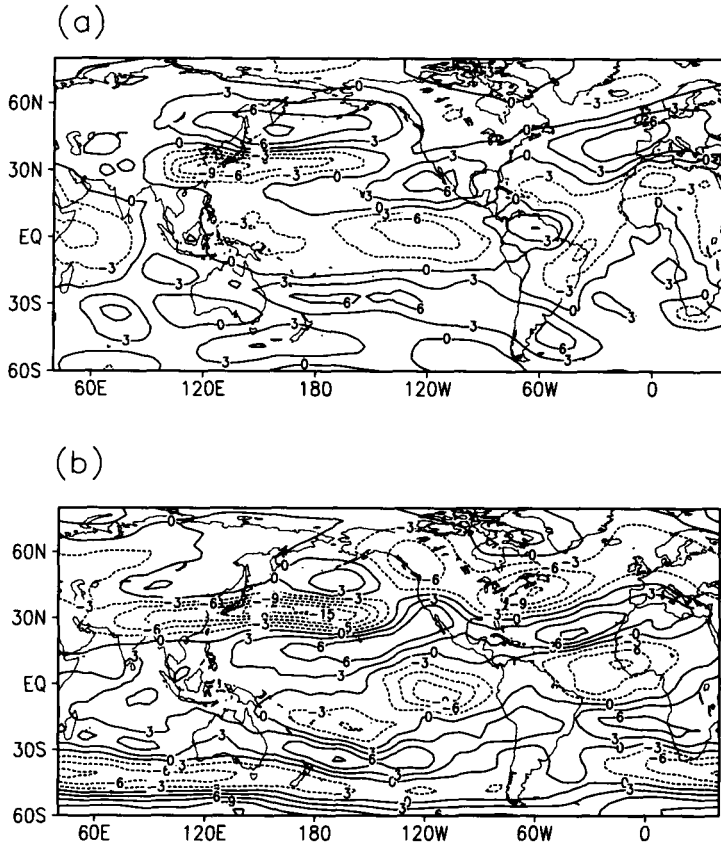


Figure 10. 200 hPa zonal wind fields. (a) Systematic error of the European Centre for Medium-Range Weather Forecasts (ECMWF) winter ensembles in January, February and March, (b) difference between March-minus-January climatology, and ECMWF re-analysis data. Contour interval 3 m s^{-1} .

south-east Asia, which (especially for divergence) are well reproduced by the ECMWF simulations. Both theoretical and modelling studies (e.g. Sardeshmukh and Hoskins 1988; Ferranti *et al.* 1994a) indicate that changes in diabatic forcing and in the divergent circulation in the west Pacific may have a strong impact on the circulation over the whole northern hemisphere. Nigam and Lindzen (1989) suggested that even minor changes in the position of the sub-tropical jet, caused by variations in the intensity of the Hadley circulation, modify both the orographic forcing arising from the interaction of the jet with the south Asian topography, and the refractive index for planetary waves which determines the propagation of the response to such forcing. Figure 11, which shows the analysis and model composites of 200 hPa zonal-wind anomalies in the Asian/west Pacific sector associated with EOF4, confirms the relationship between the divergence anomalies in Figs. 7(c) and (d) and anomalies in the strength and position of the east Asian jet. The fact that the model wind pattern is shifted to the north with respect to the analysis is consistent with the northward shift of the Pacific jet maximum, caused by the systematic error of the model (see Fig. 10(a)).

So, the EOF4 anomalies might actually result from differences in the planetary-wave forcing and propagation in the Asian sector, with the tropical anomaly acting primarily as a 'modulator' of the jet structure in the region, rather than as a direct wave source. On

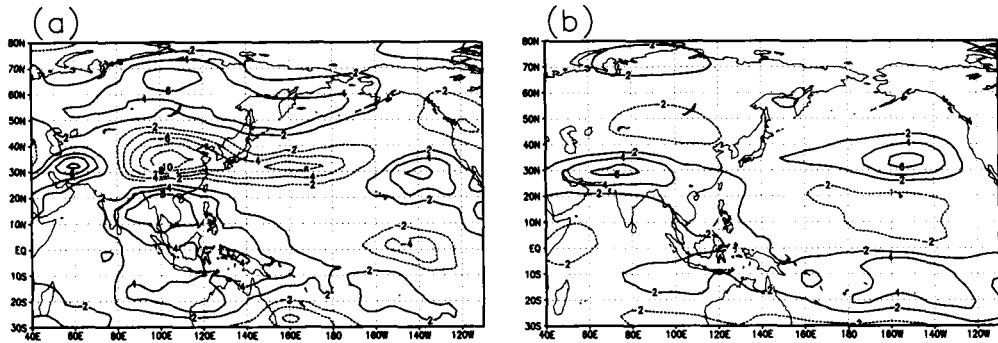


Figure 11. Composite anomalies of 200 hPa zonal wind associated with the fourth empirical orthogonal function, for (a) European Centre for Medium-Range Weather Forecasts (ECMWF) re-analysis (ERA), and (b) ECMWF ensembles. Contour interval 2 m s^{-1} . Composites are defined as in Fig. 6.

the other hand, the structure of EOF2, as shown in the composite of Fig. 6(c), suggests that a primary wave train, covering the PNA sector along a great-circle path, is connected to a secondary wave pattern originating in the tropical Atlantic, which propagates into the extra-tropical Euro–Atlantic sector.

To test the plausibility of these hypotheses, the generalized E–P flux (or wave-action flux) for stationary waves defined by Plumb (1985; see Eqs. (1) and (2)) was computed from each monthly mean of 200 hPa wind in the re-analysis dataset. The contributions of the climatological stationary waves, the linear interaction between the climate and the anomaly, and the nonlinear contribution of the wind anomaly were separately evaluated. The last term, which is independent from the sign of the anomaly, can be seen as an approximation of the total wave flux in cases of very large anomalies.

Composites of the nonlinear wave-action flux (in months when the absolute value of either PC2 or PC4 exceeded 0.67) are shown in Fig. 12 for EOF2 and EOF4, superimposed onto the eddy component of the composite geopotential anomaly. For EOF2 it is evident that the wave action is propagating from the tropics into the extra-tropics in the eastern Pacific region, and then from North America into the Caribbean region. Then, the wave-action flux is again northward in the western Atlantic between 30°N and 45°N , suggesting a reflection of the anomalous wave pattern which may be explained by the nonlinear theory of Brunet and Haines (1996).

Conversely, the wave-action flux associated with EOF4 is much more zonally oriented. While the EOF2 composite has almost no signal in the east Asian sector, a northward flux is present in that region for EOF4. On the other hand, the northward component of the flux in the east Atlantic is much weaker for EOF4 than for EOF2. If, as the wave-action flux suggests, planetary-wave reflection in the sub-tropical Atlantic affects EOF2 much more than EOF4, the sensitivity of the propagation/reflection process to the detailed structure of the zonal wind in the region (and to the implied potential-vorticity gradients) may explain why the El Niño response along EOF2 is so dependent on the phase of the seasonal cycle, and so affected by systematic errors in model simulations.

Therefore, a proper simulation of the dynamical factors which determine either the extra-tropical confinement of planetary waves, or their propagation (and eventual reflection) in the tropical Atlantic, is crucial for a successful simulation of the response to ENSO events over the Euro–Atlantic region. The relevance of the dynamics of planetary-wave propagation is further illustrated by two case studies of monthly mean

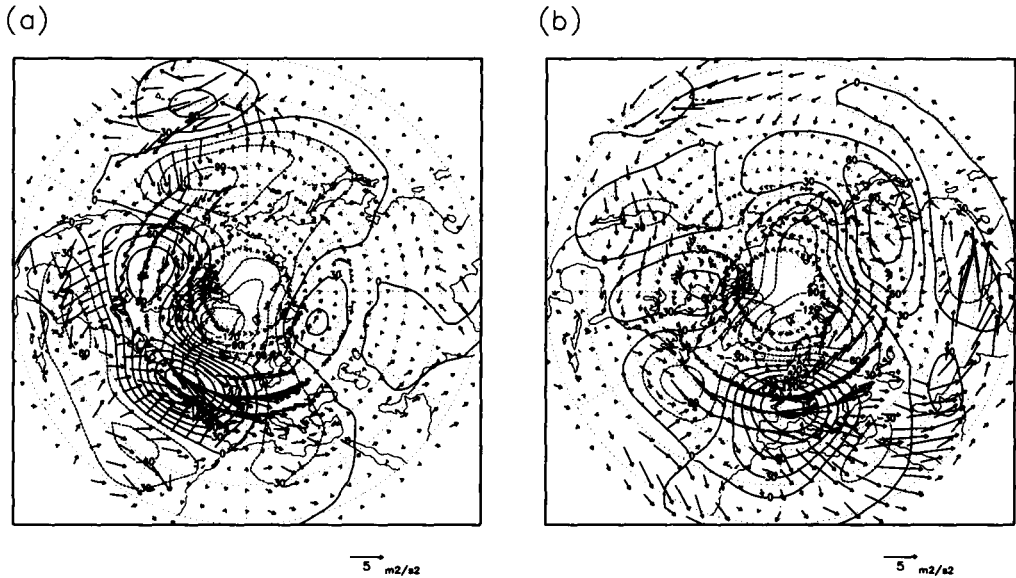


Figure 12. Composites of the nonlinear component of the generalized Eliassen–Palm flux (m^2s^{-2}), computed from European Centre for Medium-Range Weather Forecasts re-analysis fields of 200 hPa wind and geopotential height (arrows), superimposed onto the corresponding eddy anomalies of 500 hPa height (contours every 30 m). (a) Second empirical orthogonal function (EOF) composite, and (b) fourth EOF composite.

anomalies during strong El Niño events, namely in February 1983 and in January 1992. (Here, we use monthly rather than seasonal means to avoid an excessive smoothing of the dynamical fields involved in the computation of nonlinear indices.) Figures 13 and 14 show, in panel (a), the total wave-action flux computed from the 200 hPa flow from the re-analysis, superimposed onto the geopotential eddies. Panel (b) shows the ensemble-mean simulation of the same quantities, while panel (c) compares profiles of the refractive index for planetary waves computed according to Eq. (3) in the EOF domain (90°W to 60°E), from ERA and from each individual ensemble member (the ensemble-mean profile is also plotted). Note that all nonlinear diagnostics are first computed from each individual experiment and then averaged to compute the ensemble-mean fields.

The better simulation of geopotential eddies in January 1992 than in February 1983 has a counterpart in the close similarity between the observed and modelled wave-action fluxes. More interesting to note is the correspondence between errors in the wave structure and in the zonally averaged refractive index. In February 1983, the complex profile of the observed refractive index indicates a regional confinement of zonal wave-numbers two and three in a latitude band centred around 50°N , while no such confinement is present in the much smoother profile of the ensemble members. In the same month, the zonal wave-number-three eddy pattern covering the Atlantic is much underestimated in its intensity by the ensemble. In January 1992, a high-latitude confinement of zonal wave-number three is implied by the observed profile of the refractive index. This feature is reproduced by most of the ensemble members, although it is shifted about 10° southwards in the ensemble mean with respect to the analysis. Correspondingly, the eddy field is better simulated in both amplitude and zonal phase than in the previous case, but, in the ensemble the maximum of the east Atlantic positive anomaly is shifted 10° south of the observed position.

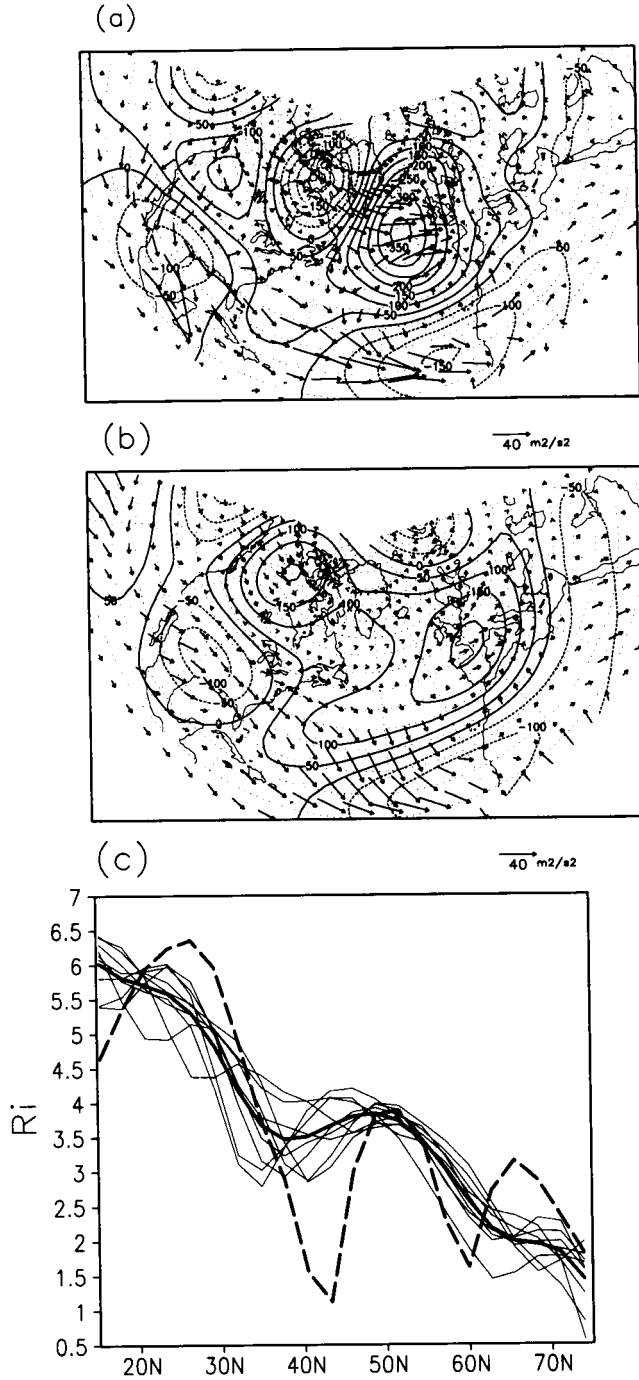


Figure 13. Planetary-wave indices for February 1983. (a) Total generalized Eliassen–Palm flux (arrows) and eddy 500 hPa height (contours every 50 m) from European Centre for Medium-Range Weather Forecasts re-analysis (ERA), (b) as in (a) but averaged over the nine members of the 1982/83 ensemble, (c) refraction index (Ri) for stationary waves from ERA (thick dashed line), from ensemble members (thin solid lines) and ensemble mean of the refraction index (thick solid line).

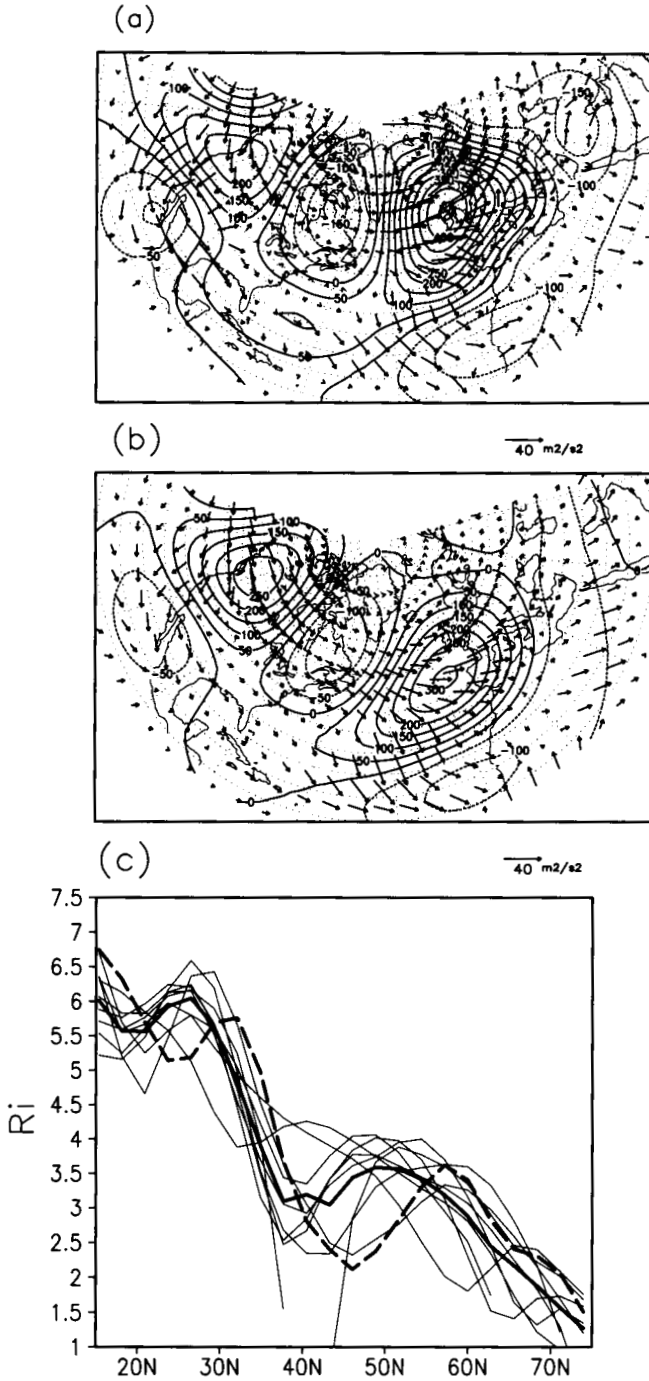


Figure 14. As Fig. 13 but for January 1992.

7. SUMMARY AND CONCLUSIONS

An EOF decomposition of wintertime monthly means of 500 hPa height (1946–94) was used to describe the interannual variability of the large-scale flow in the Euro–Atlantic region. The first four EOFs, which explain, respectively, 37%, 17%, 12% and 10% of the total variance, resemble previously documented variability patterns such as the NAO (EOF1), the eastern Atlantic pattern (EOF2), a European blocking anomaly (EOF3), and the Scandinavian pattern (EOF4).

EOF2 and EOF4 are associated with the occurrence of El Niño-like SST anomalies according to ERA and NCEP data; for EOF4, correlations with SST anomalies in the west Pacific are also important. Indications of an influence of tropical SST anomalies on the blocking-like EOF3, emerging from ERA data, are not confirmed by the NCEP multi-decadal SST record. A negligible correlation exists between EOF1 and El Niño indices during the ERA period, although a link may be detected in earlier decades.

These EOFs were used to validate a set of 14 ensembles of seasonal simulations forced by observed SSTs, performed with the ECMWF GCM as part of the PROVOST project. The best correlation (69%) between observed and ensemble-mean projections of seasonal anomalies onto the four patterns is obtained for EOF4, with the second best result (33%) for the NAO-like EOF1. For the NAO index, the level of correlation is broadly consistent with results from multi-decadal simulations by Davies *et al.* (1997) and Rodwell *et al.* (1999), and supports the hypothesis that the effects of NAO forcing by extra-tropical SSTs are more evident on interdecadal than on intradecadal variations. If, instead of the time correlation of PC time series, one considers the spatial correlation of observed and modelled composites of 500 hPa height associated with the EOFs, the NAO-like EOF1 emerges as the best simulated pattern in the Atlantic sector.

The failure of the ECMWF ensembles to simulate the interannual variability of EOF3 is not surprising if one assumes that SST anomalies have little influence on the dynamics of Euro–Atlantic blocking. However, a strong bias is present in the model simulations of this pattern, and it cannot be ruled out that model deficiencies prevent the simulation of a possible modulation of blocking frequency by boundary forcing.

On the other hand, the lack of correlation between observed and modelled variations of EOF2 is more difficult to explain, given the correlation of the observed PC2 with ENSO-related SST anomalies, and the skilful model simulations of related anomalies of rainfall and divergence in the central tropical Pacific. The analysis of dynamically oriented diagnostics, such as the wave-action flux and refractive index for stationary waves, suggests that an accurate representation of reflection and confinement of planetary waves in the Euro–Atlantic sector is essential to reproduce the regional response to ENSO-related SST anomalies. Wave reflection in the sub-tropical Atlantic seems to be particularly important for EOF2 anomalies. The inability of the ECMWF ensembles to reproduce the interannual variability of such a pattern may, therefore, be caused by an incorrect simulation of the dynamical factors which control the reflection process in the Atlantic region, such as the sub-tropical gradient of potential vorticity. The seasonality in the observed relationship between El Niño and EOF2 may also be explained by the sensitivity of this pattern to the structure of the climatological flow.

Finally, the high predictability of EOF4 seems to arise from its association with variations in the intensity and position of the Asian–Pacific jet, which in turn are controlled by west Pacific SST anomalies through a modulation of the Hadley circulation in the region. The importance of this particular anomaly pattern in setting the land-surface conditions over Eurasia at the end of winter has been analysed by Corti *et al.* (2000), and is also the subject of current numerical investigations.

ACKNOWLEDGEMENTS

The authors are grateful to the Editor and two anonymous reviewers for their useful suggestions. This work was supported by the Commission of the European Communities under project ENV4-CT95-0109.

REFERENCES

- Andrews, D. G. and McIntyre, M. E. 1976 Planetary waves in horizontal and vertical shear: The generalized Eliassen-Palm relation and the mean zonal acceleration. *J. Atmos. Sci.*, **33**, 2031-2048
- Barnston, A. G. and Livezey, R. E. 1987 Classification, seasonality and persistence of low-frequency atmospheric circulation patterns. *Mon. Weather Rev.*, **115**, 1083-1126
- Battisti, D. S., Bhatt, U. S. and Alexander, M. A. 1995 A modelling study of the interannual variability in the wintertime North Atlantic Ocean. *J. Climate*, **8**, 3067-3083
- Branković, Č. and Molteni, F. 1997 Sensitivity of the ECMWF model wintertime climate to model formulation. *Clim. Dyn.*, **13**, 75-101
- Branković, Č. and Palmer, T. N. 2000 Seasonal skill and predictability of ECMWF PROVOST ensembles. *Q. J. R. Meteorol. Soc.*, **126**, 2035-2067
- Branković, Č., Palmer, T. N. and Ferranti, L. 1994 Predictability of seasonal atmospheric variations. *J. Climate*, **7**, 217-237
- Brunet, G. and Haynes, P. H. 1996 Low-latitude reflection of Rossby wave trains. *J. Atmos. Sci.*, **53**, 482-496
- Cayan, D. R. 1992 Latent and sensible heat flux anomalies over the northern ocean: Driving the sea surface temperature. *J. Phys. Oceanogr.*, **22**, 859-881
- Corti, S., Molteni, F. and Branković, Č. 2000 Predictability of snow-depth anomalies over Eurasia and associated circulation patterns. *Q. J. R. Meteorol. Soc.*, **126**, 241-262
- Corti, S., Molteni, F. and Palmer, T. N. 1999 Signature of recent climate change in frequencies of natural atmospheric circulation regimes. *Nature*, **398**, 799-803
- Davies, J. R., Rowell, D. P. and Folland, C. K. 1997 North Atlantic and European seasonal predictability using ensembles of multidecadal atmospheric GCM simulations. *Int. J. Climatol.*, **17**, 1263-1284
- Delworth, T., Manabe, S. and Stouffer, R. J. 1993 Interdecadal variations of the thermohaline circulation in a coupled ocean-atmosphere model. *J. Climate*, **6**, 1993-2011
- Deser, C. and Blackmon, M. L. 1993 Surface climate variations over the North Atlantic Ocean during winter: 1900-1989. *J. Climate*, **6**, 1743-1753
- Deser, C. and Timlin, M. S. 1997 Atmosphere-ocean interactions on weekly timescales in the North Atlantic and Pacific. *J. Climate*, **10**, 393-408
- Ferranti, L., Molteni, F. and Palmer, T. N. 1994a Impact of localized and extra-tropical SST anomalies in ensembles of seasonal GCM integrations. *Q. J. R. Meteorol. Soc.*, **120**, 1613-1645
- Ferranti, L., Molteni, F., Branković, Č. and Palmer, T. N. 1994b Diagnosis of extra-tropical variability in seasonal integrations of the ECMWF model. *J. Climate*, **7**, 849-868
- Fraedrich, K. and Muller, K. 1992 Climate anomalies in Europe associated with ENSO extremes. *Int. J. Climatol.*, **12**, 25-31
- Gibson, J. K., Källberg, P., Uppala, S., Hernandez, A., Nomura, A. and Serrano, E. 1997 *ECMWF re-analysis. Project report series. 1. ERA description.* Eds. European Centre for Medium-Range Weather Forecasts
- Grötzner, A. M., Latif, M. and Barnett, T. P. 1998 A decadal climate cycle in the North Atlantic ocean as simulated by the ECHO coupled GCM. *J. Climate*, **11**, 831-847
- Held, I. M. 1983 Stationary and quasi-stationary eddies in the extratropical troposphere: Theory. Pp. 127-168 in *Large-scale dynamical processes in the atmosphere.* Eds. B. J. Hoskins and R. P. Pearce, Academic Press, London, UK
- Hoskins, B. J. and Karoly, D. J. 1981 The steady linear response of a spherical atmosphere to thermal and orographic forcing. *J. Atmos. Sci.*, **38**, 1179-1196
- Hurrell, J. W. 1995 Decadal trends in the North Atlantic Oscillation: Regional temperatures and precipitation. *Science*, **269**, 676-679
- 1996 Influence of variations in extratropical wintertime teleconnections on northern hemisphere temperatures. *Geophys. Res. Lett.*, **23**, 665-668

- Hurrell, J. W. and van Loon, H. 1997 Decadal variations in climate associated with the North Atlantic oscillation. *Clim. Change*, **36**, 301–326
- Kushnir, Y. 1994 Interdecadal variations in North Atlantic sea surface temperature and associated atmospheric conditions. *J. Climate*, **7**, 141–157
- Latif, M. and Barnett, T. P. 1994 Causes of decadal variability over the North Pacific and North America. *Science*, **266**, 634–637
- Latif, M., Grötzner, A., Münnich, M., Maier-Reimer, E., Venzke, S. and Barnett, T. P. 1996 A mechanism for decadal climate variability. Pp. 263–292 in *Decadal climate variability. Dynamics and predictability*. Eds. D. L. T. Anderson and J. Willebrand, Springer-Verlag, Berlin, Germany
- Molteni, F. and Corti, S. 1998 Long-term fluctuations in the statistical properties of low-frequency variability: Dynamical origin and predictability. *Q. J. R. Meteorol. Soc.*, **124**, 495–526
- Molteni, F., Tibaldi, S. and Palmer, T. N. 1990 Regimes in the wintertime circulation over northern extratropics. I: Observational evidence. *Q. J. R. Meteorol. Soc.*, **116**, 31–67
- Molteni, F., Ferranti, L., Palmer, T. N. and Viterbo, P. 1993 A dynamical interpretation of the global response to equatorial Pacific SST anomalies. *J. Climate*, **6**, 777–795
- Moura, A. D. and Shukla, J. 1981 On the dynamics of droughts in Northeast Brazil: Observations, theory and numerical experiments with a general circulation model. *J. Atmos. Sci.*, **38**, 2653–2675
- Nigam, S. and Lindzen, R. S. 1989 The sensitivity of stationary waves to variations in the basic state zonal flow. *J. Atmos. Sci.*, **46**, 1746–1768
- Palmer, T. N. and Anderson, D. L. T. 1994 The prospects for seasonal forecasting—A review paper. *Q. J. R. Meteorol. Soc.*, **120**, 755–793
- Palmer, T. N. and Sun, Z. 1985 A modelling and observational study of the relationship between sea surface temperature anomalies in the north-west Atlantic and the atmospheric general circulation. *Q. J. R. Meteorol. Soc.*, **111**, 947–975
- Parker, D. E., Folland, C. K., Bevan, A., Ward, M. N., Jackson, M. and Maskell, K. 1995 Marine surface data for analysis of climate fluctuations on interannual to century timescales. *Natural climate variability on decade-to-century timescales*. Eds. D. G. Marthinson, K. Bryan, M. Ghil, M. M. Hall, T. R. Karl, E. S. Sarachick, S. Sorooshian and L. D. Talley, National Research Council, National Academy Press, Washington, D.C., USA
- Pavan, V., Tibaldi, S. and Branković, Č. 2000 Seasonal prediction of blocking frequency: Results from winter ensemble experiments. *Q. J. R. Meteorol. Soc.*, **126**, 2125–2142
- Peng, S., Mysak, L. A., Ritchie, H., Derome, J. and Dugas, B. 1995 The differences between early and midwinter atmospheric responses to sea surface temperature anomalies in the north-west Atlantic. *J. Climate*, **8**, 137–157
- Plumb, R. A. 1985 On the three-dimensional propagation of stationary waves. *J. Atmos. Sci.*, **42**, 217–229
- Rao, V. B., de Lima, M. C. and Franchito, S. H. 1993 Seasonal and interannual variations of rainfall over eastern north-east Brazil. *J. Climate*, **6**, 1754–1763
- Ratcliff, R. A. S. and Murray, R. 1970 New lag associations between North Atlantic sea temperature and European pressure applied to long-range weather forecasting. *Q. J. R. Meteorol. Soc.*, **96**, 226–246
- Reynolds, R. W. and Smith, T. M. 1994 Improved global sea surface temperature analysis using optimum interpolation. *J. Climate*, **7**, 929–948
- Rodo', X., Baert, E. and Comin, F. A. 1997 Variations in seasonal rainfall in Southern Europe during the present century: Relationships with the North Atlantic Oscillation and the El-Niño–Southern Oscillation. *Clim. Dyn.*, **13**, 275–284
- Rodwell, M. J., Rowell, D. P. and Folland, C. K. 1999 Oceanic forcing of the wintertime North Atlantic Oscillation and European climate. *Nature*, **398**, 320–323
- Rogers, J. C. 1990 Patterns of low-frequency monthly sea level pressure variability (1899–1989) and associated wave cyclone frequencies. *J. Climate*, **3**, 1364–1379
- Rowell, D. P., Folland, C. K., Maskell, K. and Ward, M. N. 1995 Variability of summer rainfall over tropical North Africa (1906–1992): Observations and modelling. *Q. J. R. Meteorol. Soc.*, **121**, 669–704
- Sardeshmukh, P. D. and Hoskins, B. J. 1988 Generation of global rotational flow by steady idealized tropical divergence. *J. Atmos. Sci.*, **45**, 1128–1251

- Smith, T. M., Reynolds, R. W., Livezey, R. E. and Stokes, D. C. 1996 Reconstruction of historical sea surface temperatures using empirical orthogonal functions. *J. Climate*, **9**, 1403–1420
- Tibaldi, S. and Molteni, F. 1990 On the operational predictability of blocking. *Tellus*, **42A**, 343–365
- Tibaldi, S., Tosi, E., Navarra, A. and Pedulli, L. 1994 Northern and southern hemisphere seasonal variability of blocking frequency and predictability. *Mon. Weather Rev.*, **122**, 197–200
- Valero, F., Doblas, F. J. and Gonzalez, J. F. 1996 On long-term evolution of seasonal precipitation in southwestern Europe. *Annales Geophysicae*, **14**, 976–985
- Van Loon, H. and Rogers, J. C. 1978 The seesaw in winter temperature between Greenland and Northern Europe. Part I: General description. *Mon. Weather Rev.*, **106**, 296–310
- Wallace, J. M. and Gutzler, D. S. 1981 Teleconnections in the geopotential height field during the northern hemisphere winter. *Mon. Weather Rev.*, **109**, 784–812
- Wallace, J. M. and Jiang, D. S. 1987 On the observed structure of the interannual variability of the atmosphere/ocean climate system. Pp. 17–43 in *Atmospheric and Oceanic Variability*. Ed. H. Cattle, Royal Meteorological Society
- Wallace, J. M., Smith, C. and Bretherton, C. S. 1992 Singular value decomposition of wintertime sea surface temperature and 500-mb height anomalies. *J. Climate*, **5**, 561–576
- Xie, P. and Arkin, P. A. 1996 Analyses of global monthly precipitation using gauge observations, satellite estimates and numerical model predictions. *J. Climate*, **9**, 840–858
- Zorita, E. and Frankignoul, C. 1997 Modes of North Atlantic decadal variability in the ECHAM1/LSG coupled ocean-atmosphere general circulation model. *J. Clim.*, **10**, 183–200